MASTER COPY KEEP THIS COPY FOR REPRODUCTION PURPOSES

REPORT DOCUMENTATION PAGE

Form Approved
OMB No. 0704-0188

1. AGENCY USE ONLY (Leave blank)	2. REPORT DATE	3. REPORT TYPE AND DATES COVERED
	March 13, 1995	Final Report 8/91 - 12/94

4. TITLE AND SUBTITLE
The Design and Construction of an Ion Trap Based System for Laser Pyrolysis/Mass Spectrometry of Single Organic Aerosol Particles

5. FUNDING NUMBERS
DAAL03-91-G-0296

6. AUTHOR(S)
Henk L.C. Meuzelaar
Neil S. Arnold, George Hars, Paul A. Cole

7. PERFORMING ORGANIZATION NAME(S) AND ADDRESS(ES)
Center for Micro Analysis & Reaction Chemistry
University of Utah
214 EMRL
Salt Lake City, UT 84112

8. PERFORMING ORGANIZATION REPORT NUMBER
MARC R95-001

9. SPONSORING / MONITORING AGENCY NAME(S) AND ADDRESS(ES)
U.S. Army Research Office
P.O. Box 12211
Research Triangle Park, NC 27709-2211

10. SPONSORING / MONITORING AGENCY REPORT NUMBER
ARO 29332.2-LS

11. SUPPLEMENTARY NOTES
The views, opinions and/or findings contained in this report are those of the author(s) and should not be construed as an official Department of the Army position, policy, or decision, unless so designated by other documentation.

12a. DISTRIBUTION / AVAILABILITY STATEMENT
Approved for public release; distribution unlimited.

12b. DISTRIBUTION CODE

13. ABSTRACT *(Maximum 200 words)*

A multifunction Paul trap capable of stabilizing and analyzing electrostatically charged microparticles as well as a broad range of ions and macro-ions has been developed. Typically, particles in the 0.1-10 μm range are introduced by aerosolization and a single particle is selected and stabilized under scattered light observation while the pressure is reduced to $< 10^{-5}$ torr. A new particle trajectory pattern, observed in the equatorial plane, offers a potentially new, nondestructive, optical method for determining the m/z value of microparticles and macro-ions, with a maximum theoretical accuracy of ~ $1:10^6$. Irradiation of the particle with a Nd YAG laser enables production of laser fragmentation/ionization mass spectra of 1 μm dia polystyrene particles and of *Bacillus subtilis* spores. Shot-to-shot reproducibility is still unsatisfactory, however, and mass calibration problems need to be resolved. Nonetheless, the high intensity and complex organic nature of the ion signals indicate the potentiality for chemical and physical characterization of single microorganisms and other components of respirable aerosols.

14. SUBJECT TERMS	15. NUMBER OF PAGES
	45
	16. PRICE CODE

17. SECURITY CLASSIFICATION OF REPORT	18. SECURITY CLASSIFICATION OF THIS PAGE	19. SECURITY CLASSIFICATION OF ABSTRACT	20. LIMITATION OF ABSTRACT
UNCLASSIFIED	UNCLASSIFIED	UNCLASSIFIED	UL

The Design and Construction of an Ion Trap Based System for Laser Pyrolysis/Mass Spectrometry of Single Organic Aerosol Particles

Final Report

Principal Investigator:
Henk L.C. Meuzelaar

Co-Investigators:
Neil S. Arnold
George Hars
Paul A. Cole

March 1995

U.S. ARMY RESEARCH OFFICE

Grant Number: DAAL03-91-G-0296

Center for Micro Analysis & Reaction Chemistry
University of Utah
Salt Lake City, UT 84112

THE VIEW, OPINIONS, AND/OR FINDINGS CONTAINED IN THIS REPORT ARE THOSE OF THE AUTHOR(S) AND SHOULD NOT BE CONSTRUED AS AN OFFICIAL DEPARTMENT OF THE ARMY POSITION, POLICY, OR DECISION, UNLESS SO DESIGNATED BY OTHER DOCUMENTATION.

TABLE OF CONTENTS

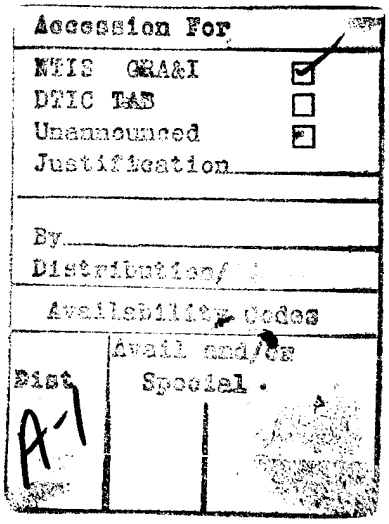

EXECUTIVE SUMMARY

Since the start of the project on August 1, 1991, all of the tasks described in the original proposal (see Table I) have been addressed successfully. However, due to the fact that years 2 and 3 were funded at a strongly reduced level, Tasks 4, 5 and 6 could only be carried out at a feasibility demonstration level. Without the ability to complete the full experimental matrix for these tasks, several issues regarding reproducibility, specificity and, in particular, applicability (viz. type of microorganisms or other aerosol components that can be analyzed with this technique) remain unanswered.

TABLE I
TIME PLAN

	Year 1				Year 2				Year 3			
Task 1: (Sample Introduction)	X	X	X	X	.	.	.	.	.	.	.	.
Task 2: (Particle Containment)	.	.	X	X	X	X	.	.	.	.	.	.
Task 3: (Imaging and Stabilization)	.	.	.	.	X	X	.	.	.	.	.	.
Task 4: (Laser Pyrolysis/Desorption)	.	.	.	.	.	X	X	X	X	.	.	.
Task 5: (MS Detection)	.	.	.	.	.	.	.	.	X	X	X	X
Task 6: (Biocompound Analysis)	.	.	.	.	.	.	.	.	.	X	X	X
Task 7: (Reporting)	.	.	.	X	.	.	.	X	.	.	.	X

In order to document the experiments carried out thus as completely as possible and lay the groundwork for future continuation, instrumental design considerations as well as underlying theoretical aspects and actual experimental observations have been discussed in a

series of articles and conference presentations (see Appendix 1). Besides confirming the overall feasibility of laser pyrolysis/ionization mass spectrometry of single organic aerosol particles by means of ion trap methods, the results of the work indicate the potential for several spin-off technologies, including precise mass determination of megadalton ions by means of nondestructive optical techniques as well as the possibility of introducing and trapping large ions produced by atmospheric pressure ionization methods, e.g., electrospray ionization. The latter topic is currently the focus of special attention as it appears to offer an opportunity for continued funding under ERDEC auspices while utilizing much of the expertise and instrumentation developed under the project described in the present report. Finally, it should be mentioned here that co-investigator, Dr. George Hars, who returned to his native country (Hungary) in 1993, has submitted a proposal to the Joint US/Hungarian fund to support the continuation of several aspects of this work at the Department of Atomic Physics, Technical University of Budapest in direct collaboration with the University of Utah Center for Micro Analysis and Reaction Chemistry.

From the work reported here, the following conclusions and recommendations can be formulated.

Conclusions:

1) Micron- and submicron-sized particles can be trapped from electrospray sources from vaporized suspensions in H_2O, or directly from air.

2) Trapped particles can be pumped down to high vacuum ($<10^{-4}$ torr) conditions without loss of stability.

3) Under high vacuum conditions particles describe a star-like pattern in the equatorial plane that can be used for precise mass/charge ratio determinations.

4) Use of a Nd YAG laser beam at 1.06 μm produces intense ion signals from single styrene particles or *B. subtilis* spores which appear to represent complex organic compounds.

Recommendations:

1) Further experiments are needed to optimize Nd YAG laser pulse intensities, beam alignment and choice of wavelengths (the 1.06 μm wavelength can be doubled, tripled or quadrupled), especially in order to increase shot-to-shot reproducibility.

2) Use of tandem MS techniques should enable identification of the presently unknown ion signals.

3) A systematic analysis of different types of aerosol particles, supported by pattern recognition methods will be needed to evaluate the applicability of the new technique to various biodetection problems.

INTRODUCTION

The development of a multifunction (electrodynamic balance + ion trap mass spectrometer) Paul trap capable of trapping, stabilizing and analyzing microparticles (ranging in size from 0.1 to several tens of microns) as well as ions (ranging in size from a few Daltons to gigaDaltons) was undertaken for the primary purpose of obtaining characteristic mass spectra of single microorganisms and other respirable aerosol particles. As reported at the 1992 ERDEC Scientific Conference[1] successful trapping and visualization of micron-, or even submicron-, sized particles injected by means of various aerosolization methods was accomplished in a modified Finnigan MAT type ion trap electrode assembly. Optimization of the trapping potential, using a square wave drive frequency, was shown to enable evacuation of the chamber to less than 10^{-4} torr without destabilizing the trapped particle. However, preliminary attempts to produce characteristic mass spectra by means of hitting the stabilized particle with the focussed beam of a small TEA CO_2 laser failed to produce adequate ion signal. Serendipitously, particles trapped at pressures $<10^{-4}$ torr were observed to exhibit a previously unreported star-shaped trajectory in the equatorial plane. This trajectory was found to be a function of m/z value.

The present report describes the evolution of a novel, nondestructive optical method for determining the mass of a single megadalton ion (or microparticle) with a potentially high degree of accuracy. Secondly, the authors report the installation of a more powerful (Nd, YAG type) laser and the results of preliminary laser fragmentation/ionization (LFI) MS studies on polystyrene microparticles and *Bacillus subtilis* spores.

EXPERIMENTAL

Instrumentation

Figure 1 shows the experimental setup. A modified Finnigan ITD 700 ion trap electrode assembly is used. The ring electrode has three radial drill holes (3 mm dia). Two are directly in line with each other, the third one is positioned at a 90 degree angle. The two aligned holes carry the HeNe laser beam through the center of the trap. The perpendicular hole is used to detect and observe particles in the center of the trap levitated by means of a long working distance optical microscope (Cohu 312985) with highly sensitive CCD camera (Cohu 6410). The camera can also be operated from a vertical position for observing the center of the trap through the central hole in the upper end cap. The ring electrode is driven with a rectangular voltage signal ranging from 500 Hz to 3 kHz in frequency and up to 2 kV in amplitude. The end cap electrodes are driven by a power supply providing both DC and/or AC modulation in common or in opposite phase mode. A UV lamp placed underneath the trap projects its light through the central hole of the lower end cap, thus illuminating the center of the trap. The pulsed beam (5 ns, 450 mJ) of the Nd-YAG laser (Continuum, Surelite J-10) is focussed to the center of the ion trap without illuminating any part of the electrode system. The trap is contained within a UHV vacuum housing with suitable view ports. The necessary pumping is provided by a 170 l/s TPU 170 Balzers turbo pump+ rotary forepump combination. During evacuation of the trap, the pressure is monitored by means of a Baratron gauge.

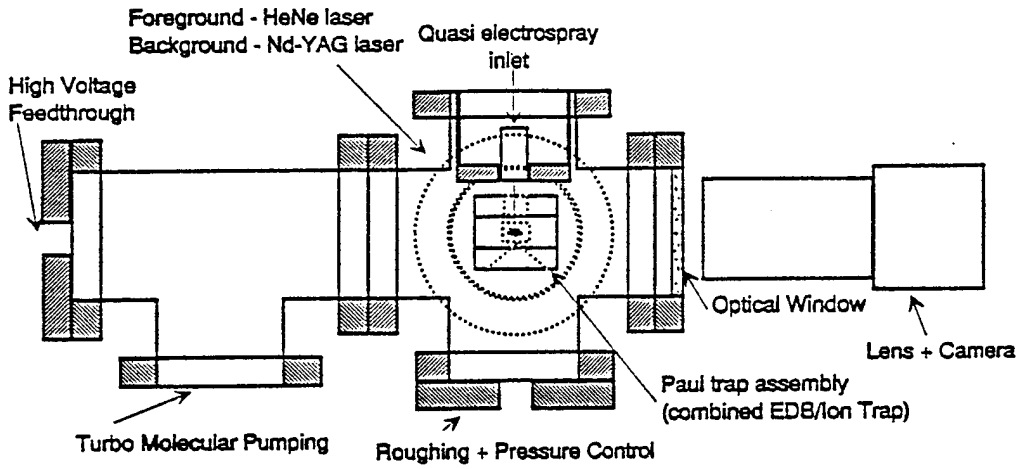

Figure 1. The experimental setup of the particle analyzer equipment.

Experimental Methods

First the particles are suspended in water and then introduced into the ion trap by means of a syringe through the central hole of the upper end cap. Because of the high electric field in the trap most of the particles will be spontaneously charged. The initial value for the mass/charge ratio is about 10^9 a.m.u./unit charge. Generally more than one particle is trapped. Particles near the center of the trap are being visualized by means of the HeNe target beam and a highly sensitive video microscopy system. Applying opposite mode DC on the end caps and gradually increasing the drive frequency of the ring results in ejecting all particles except one. This particle will be centered in the trap. Subsequently the vacuum system is gradually pumped down to $<10^{-4}$ torr. In order to avoid arcing in the trap during evacuation, a rectangular voltage signal is used to drive the ring electrode. The rectangular signal provides the highest possible trapping potential at limited (200 V) voltage amplitude at high drag conditions. Below 10^{-4} torr the particle reveals highly characteristic and stable oscillation patterns. In the equatorial plane of the ion trap the particle performs an elliptical motion. At specific voltages and frequencies the rapidly circulating particle can be observed as a quasi

standing oscillation which resembles a star pattern (see Figures 2 and 3). By counting the "branches" of the star and measuring the corresponding voltage and frequency, the mass/charge ratio of the particle can be calculated. Subsequent UV radiation to induce stepwise electron loss events enables the absolute mass of a single macro-ion in the 10^9-10^{12} Dalton range to be determined.

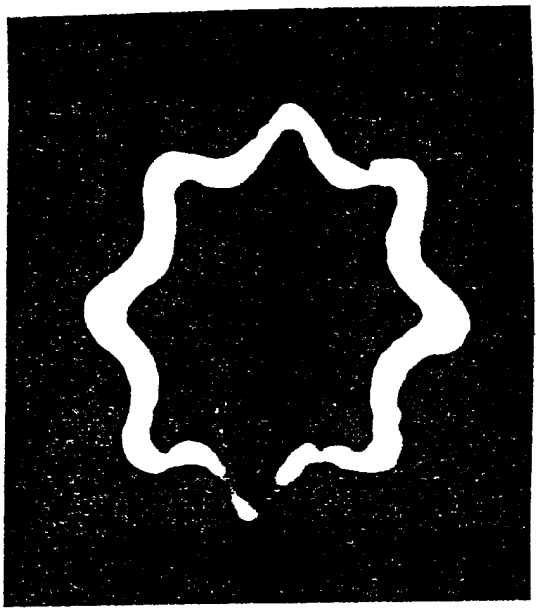

Figure 2. Eight branch star pattern of a 1.0 μm diameter polystyrene particle to the equatorial plane of the ion trap.

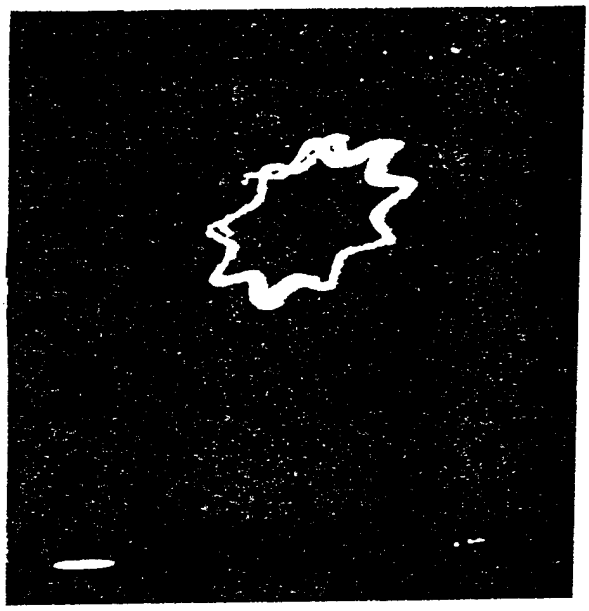

Figure 3. Nine branch star pattern of a 1.0 μm diameter *B. subtilis spore* particle in the equatorial plane of the ion trap.

Chemical characterization is performed in the same Paul trap, while operating in the Ion Trap Mass Spectrometer (ITMS) mode. Moreover, since the mass determination procedure is nondestructive, the same microparticle or macro-ion can be analyzed while still stabilized in the trap. First He buffer gas is introduced into the vacuum system to 10^{-4} torr. Because of the increased drag, the star pattern of the particle shrinks until the particle appears as a single bright dot in the center of the trap. Subsequently, the trapped particle is fragmented and ionized by means of a single, 5 ns, 450 mJ pulse from a Nd YAG laser operating at 1.06 μm. Simultaneous with the laser pulse the electronic drive of the ring electrode is switched from

the mass determination to the ITMS mode in order to record a mass spectrum of the ion fragments created by the laser shot (Figures 4 and 5).

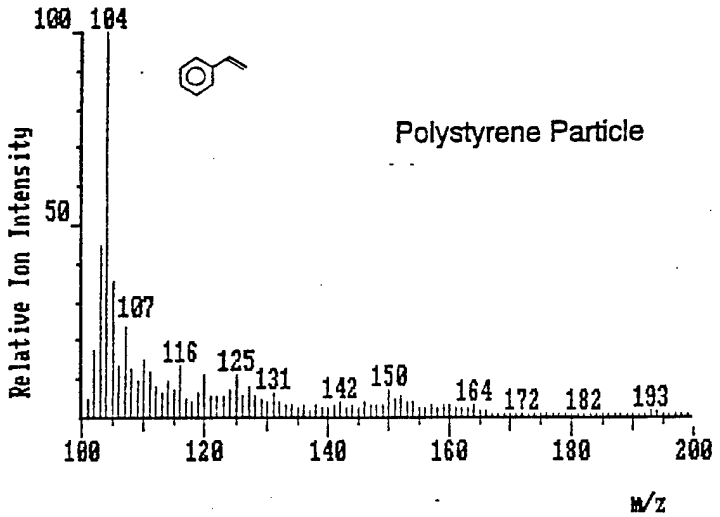

Figure 4. LFI mass spectrum of a 1 μm dia. polystyrene particle (or a small cluster of particles) showing dominant ion peak at m/z 104, believed to represent the styrene monomer unit. The pattern shown is not very reproducible in that repeat shots may show a similar ion cluster at m/z values anywhere between m/z 104 and 110.

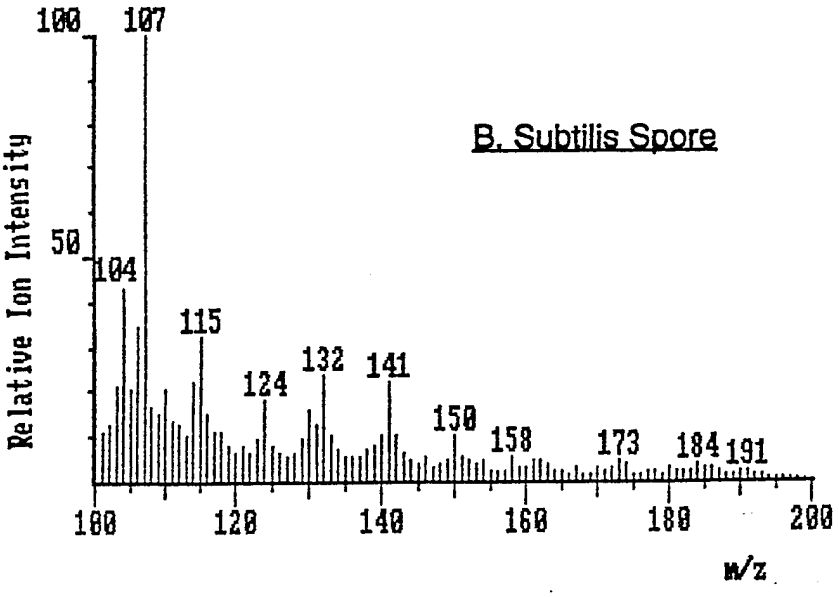

Figure 5. LFI mass spectrum of a *Bacillus subtilis* (or a small cluster of several spores) showing a more complex pattern than Figure 3. A similar type of pattern was found in about 40-50% of the *B. subtilis spore* analyses. Note frequent peak intervals of 15, 17, 18 and 26 amu, suggesting dominant organic ion signals.

RESULTS AND DISCUSSION

Mass Determination of the Particle

A theoretical discussion of the novel mass determination principle introduced here is based on the pseudo-potential model of the ion trap[2]. In this model the charged particle is considered to be in a spring-like linear force field, although the spring constants D_r and D_z are unequal. For mathematical purposes the origin of a Cartesian coordinate system is put into the center of the trap. The x and y axis are in the equatorial plane and the electrode system is rotationally symmetric around the vertical z axis. Since x and y are equivalent they will be often referred as r (standing for radial direction). The vector of average force affecting the charged particle is F.

$$F = -D_r(xi+yj) - D_z zk \qquad (1)$$

Here i, j, k are the unit vectors of the coordinate system in x, y and z directions respectively. The values of D_r and D_z are derivable from the model and are as follows:

$$D_r = \frac{1}{2m}\left(\frac{QV}{r_o^2\Omega}\right) \qquad D_z = \frac{2}{m}\left(\frac{QV}{r_o^2\Omega}\right)^2 \qquad (2)$$

where D_r and D_z are the spring constants, m and Q are the mass and charge of the particle, V and Ω are the voltage amplitude and the angular frequency of the drive and finally r_o is the radius of the ring electrode.

Apparently, the "spring" in z direction is four times stronger than in r direction. ($D_z = 4D_r$) The equation of motion can readily be solved. The x and y components are identical. The motion in each direction is a harmonic oscillation. The oscillation frequency in x,y and z directions are $\omega_x=\omega_y=\omega_r$ and ω_z respectively:

$$\omega_r = \sqrt{\frac{D_r}{m}} \qquad \omega_z = \sqrt{\frac{D_z}{m}} \tag{3}$$

These are the so-called secular frequencies. Obviously the secular frequency in z direction is twice higher. Substituting (2) into (3) the values of the secular frequencies result as:

$$\omega_r = \frac{\sqrt{2}}{2}\,\frac{QV}{m\,r_o^2\Omega} \qquad \omega_z = \sqrt{2}\,\frac{QV}{m\,r_o^2\Omega} \tag{4}$$

So far the average force affecting the particle was considered to be a function of position only. In reality this average force is the result of several "pushes and pulls" so the trajectory of the particle shows a fine structure which is synchronous with the drive frequency. If the drive frequency/secular frequency ratio is an integer then the fine structure on the trajectory will seem to be standing. In the case of the elliptical motion in the equatorial plane the fine structure due to drive frequency will result in a standing star pattern provided that the star pattern condition is met:

$$n\ \omega_r = \Omega \tag{5}$$

$$\frac{m}{Q} = \frac{\sqrt{2}}{2}\,\frac{n\,V}{r_o^2\,\Omega^2} \tag{6}$$

where n is an integer. From (5) the mass/charge ratio of the particle can readily be expressed: The value of n can be obtained by counting the branches of the star. By means of (6) the mass/charge ratio can be determined by adjusting a standing (mostly eight branch) star pattern and by measuring the voltage and the frequency of the corresponding drive.

Illuminating the negatively charged particle with very faint UV light the electrons will be removed from the particle one by one[3]. Some second succession can be readily adjusted by using faint enough UV light. If the particle to be analyzed is in a standing star pattern the loss of electrons will cause the pattern to spin again. Then the pattern can be stabilized by reducing the drive frequency. The mass/charge ratios before and after the electron loss can be expressed by means of (6):

$$\frac{m}{Z\,e} = \frac{\sqrt{2}}{2}\,\frac{n\,V}{r_o^2\,\Omega_1^2} \qquad\qquad \frac{m}{(Z\text{-}1)e} = \frac{\sqrt{2}}{2}\,\frac{nV}{r_o^2\,\Omega_2^2} \tag{7}$$

where Z is the ionization level, e is the elemental charge 1.6×10^{-19} as, Ω_1 and Ω_2 are neighbor drive frequencies. The absolute mass can be calculated from (7):

$$m = \frac{\sqrt{2}}{2}\,\frac{n\,V\,e}{r_o^2\,(\Omega_1^2 - \Omega_2^2)} \tag{8}$$

Since the particle carrier at least several hundred unit charges the measurement can be repeated a number of times, thus making the method more dependable.

Laser Fragmentation/Ionization MS

The LFI mass spectrum of a 1.0 μm polystyrene particle illustrated in Figure 4 is characterized by the occurrence of mass peaks at every nominal m/z value within the selected mass range. Furthermore, the mass intensities are quite high (typically 10^5-10^6 "ion counts" full scale). Finally, the spectrum appears to be dominated by organic compound signals in view of the frequent occurrence of 14, 15 or 28 amu intervals rather than the m/z 23 or 39 intervals characteristic of sodium and potassium ion contributions or the 12 amu intervals associated with carbon cluster formation. Unfortunately, detailed chemical interpretation of the mass spectrum in Figure 3 is presently impossible since the signals do not directly correspond to the

expected styrene and styrene-like decomposition products. The most likely explanation is that the high initial concentrations of ions in the ion trap are causing significant shifts in the mass scale calibration. Similarly, the *B. subtilis* spore spectrum in Figure 5 also provides high ion intensities combined with a current lack of biochemical interpretability. Complex secondary reactions, e.g., due to excessive laser intensities and/or an unknown mass scale calibration shifts due to space charge phenomena in the trap may well be responsible for these problems. Before any detailed conclusions can be drawn, however, it will be necessary to confirm the organic nature and information content of the ion signals observed. Since the ion trap system can be operated in a tandem MS mode it should be possible to produce daughter ion spectra and thus identify some of the major peak signals in Figures 4 and 5.

ACKNOWLEDGEMENTS

The authors want to acknowledge helpful advice from Randy Long and Robert McLane, as well as the expert technical assistance of Paul Cole.

REFERENCES

1. Arnold, N.S.; Hars, G.; Cole, P.A.; Meuzelaar, H.L.C., Proc. 1992 US Army ERDEC Scientific Conference, 1993, 219.

2. Wuerker,R.F.; Shelton,H.; Langmuir,R.V. J.Appl.Phys. 30(3), 1959, 342.

3. Arnold, S.J., Aerosol Sci., 10, 1979, 49.

APPENDIX I

Articles, Presentations and Proposals Directly Resulting from the Work Reported Here:

1. Arnold, N.S., Hars, G., Cole, P.A., Meuzelaar, H.L.C. "Development of a Single Chamber EDB/ITMS System for Laser Pyrolysis MS Analysis of Individual Microparticles," Proceedings of the 1992 U.S. Army ERDEC Scientific Conference on Chemical Defense Research, November 17-20, 1992, Aberdeen Proving Grounds, MD, 1993, ERDEC-SP-007, 219-225 (copy included)

2. Hars, G., Arnold, N.S., Meuzelaar, H.L.C., "Mass Determination of Trapped Micro-Particles and Macro-Ions by Optical Techniques (and Subsequent Chemical Analysis by Laser Pyrolysis Mass Spectrometry)," Proceedings of the 41st ASMS Conference on Mass Spectrometry and Allied Topics, June 1-4, 1993, San Francisco, CA, 1993, 800 (copy included).

3. Arnold, N.A., Hars, G., Meuzelaar, H.L.C., "Chemical Characterization of Single Aerosol Particles Via Combined Electrodynamic Balance/Ion Trap Mass Spectrometry Techniques," ACS Preprints, Chicago, IL, August 1993 (abstract only, included).

4. Hars, G., Arnold, N.S., Meuzelaar, "Chemical Characterization of Single Aerosol Particules Via Combined Electrodynamic Balance/Ion Trap Mass Spectrometry Techniques," Proceedings of the 1993 U.S. Army ERDEC Scientific Conference on Chemical Defense Research, November 16-19, 1993, Aberdeen Proving Grounds, MD, 1994, ERDEC-SP-024, 177-183 (copy included).

5. Arnold, N.S., Hars, G., Meuzelaar, H.L.C., "Extended Theory of Mass Resolution for Resonance Ejection Quadrupole Ion Trap Mass Spectrometry," Journal of the American Society for Mass Spectrometry, 1994, 5, 676-688 (copy included).

6. Hars, G., Arnold, N.S., Meuzelaar, H.L.C., "A New Method for Precise Mass Determination of Charged Micron and Submicron Size Particles by Combined Paul Trapping and Optical Detection Techniques," *Rev. Sci. Insts.* submitted (upon publication, copies will be sent to US Army).

7. Hars, G., "Some Theoretical and Practical Aspects of Ion Trap Physics with a Special Respect to the Accurate Mass Determination of Some Submicron Size Charge Particles,"Thesis, Technical University of Budapest, Hungary, in press (upon publication, copies will be sent to US Army).

8. Proposal to Joint U.S./Hungarian Fund, "Aerosol Characterization by Means of the Quadrupole Ion Trap," 1994, submitted (copy of statement of work attached).

EDGEWOOD
RESEARCH,
DEVELOPMENT &
ENGINEERING
CENTER

ERDEC-SP-007

PROCEEDINGS
OF THE 1992 ERDEC
SCIENTIFIC CONFERENCE ON CHEMICAL DEFENSE RESEARCH
17-20 NOVEMBER 1992

Joseph D. Williams, Jr.
Dorothy A. Berg
Patricia J. Reeves

RESEARCH AND TECHNOLOGY DIRECTORATE

June 1993

U.S. ARMY
CHEMICAL
AND BIOLOGICAL
DEFENSE AGENCY

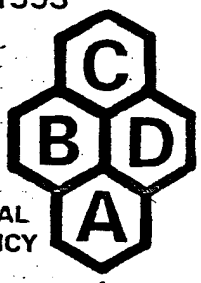

Aberdeen Proving Ground, Maryland 21010-5423

DEVELOPMENT OF A SINGLE CHAMBER EDB/ITMS SYSTEM FOR LASER PYROLYSIS MS^n ANALYSIS OF INDIVIDUAL MICROPARTICLES

Neil S. Arnold, György Hars*, Paul A. Cole and
Henk L.C. Meuzelaar

Center for Micro Analysis & Reaction Chemistry
University of Utah
Salt Lake City, UT 84112

* on leave from TU-Budapest, 1111 HUNGARY

ABSTRACT

A novel technique for laser mass spectrometry of individual particles, e.g. microorganisms, is being developed. Present paper gives a detailed discussion on the theoretical and experimental aspects of trapping a submicron size charged particles pressures from atmospheric down to $<10^{-7}$ torr. The ability to trap particles under UHV conditions has provided a new opportunity to study "ion trajectories" as they perform the solution of Mathieu equation.

Individual microparticles, mainly microorganisms, have been aerosolized and charged by a quasi-electrospray technique. A Paul type three-dimensional quadrupole "trap" was constructed to combine the properties of an EDB (Electro-Dynamic Balance)[1], capable of capturing and stabilizing micro-sized particles, with those of an ITMS (Ion Trap Mass Spectrometer), capable of trapping and mass selectively detecting ionic species up to several thousand amu[2,3]. A TEA CO_2 laser (300 mJ per 200 μsec pulse) with focussing optics designed to produce a 50-80 μm beam waist through the center of the trap is used. A typical analysis cycle starts with the trap in EDB mode, thereby enabling capture and stabilization of one or more particles, followed by evacuation of the trap to high vacuum ($<10^{-3}$ torr).

Subsequently, pyrolysis/desorption/ionization of the trapped particles will be performed with a single CO_2 laser pulse while switching the trap over to ITMS mode, thereby enabling mass selective analysis of the ionic species produced, including quasimolecular (e.g., cationized[4]) species. The present paper presents interim results on ionization and stabilization of the individual organic and biological particles.

INTRODUCTION

Previous work in our laboratory has established the feasibility of CO_2 laser pyrolysis of individual, 50-100 μm dia. microparticles suspended (levitated) in the center of an electrodynamic balance (EDB) chamber at ambient pressure, followed by GC/MS analysis of the pyrolysis vapor products with an ion trap mass spectrometer (ITMS) system at high vacuum[5]. A 2 m long, 180 μm i.d. transfer line GC column connecting the EDB and ITMS chambers functions both as a pressure reducer and, via ballistic heating, as a temperature programmed GC column. Both the EDB and the ITMS cell are Paul-type, RF-only traps operating in different experimental regimes. In order to investigate the feasibility of analyzing single particles in the 1-50 μm range while eliminating transmission losses between the two cells, a fully integrated chamber, performing both EDB and ITMS functions was constructed (see Figure 1). Major experimental challenges are: (1) to quickly stabilize the particles under high vacuum conditions; (2) to pyrolyze these particles with a short CO_2 laser pulse; and (3) to efficiently trap ionized laser pyrolysis products.

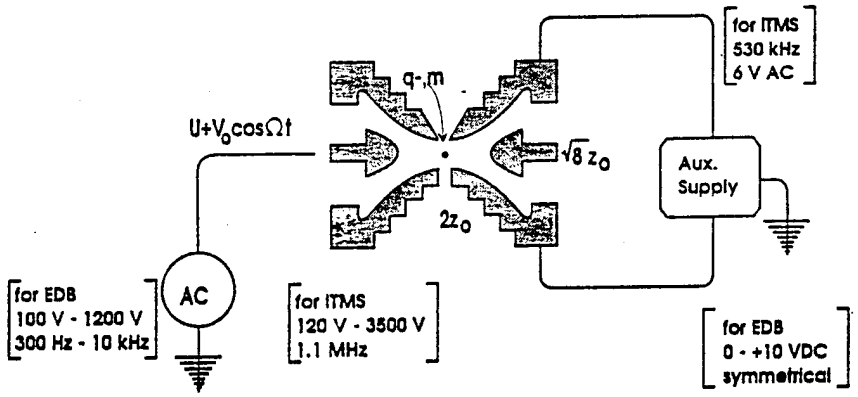

Figure 1. Typical electrical conditions for EDB and ITMS trap operation.

EXPERIMENTAL

A schematic of the particle levitation apparatus, as presently conceived, is displayed in Figure 2. Sample introduction is from the top of the trap via electrospray from a MeOH solution. HeNe laser illumination projects into the page while the CO_2 laser path will be into the trap from the opposite side. Particles are detected via scattering through a 3 mm hole in the ring electrode using a Lieca MonoZoom 7 lens and Cohu 6400 series CCD camera. The vacuum system is pumped by a 110 l/s Balzer turbo molecular pump.

The electrospray injector was constructed from a syringe and a high voltage power supply. A 26.5 ga needle, cut off and polished, formed the spray tip and particles were introduced into the syringe as a suspension in methanol (typically 2.5 x 10^{-2} weight %). The needle tip was connected via a 20 M Ω current limiting resistor to the high voltage (-3 to +3 KV) power supply while the electrically insulated plunger was operated manually via light tapping to eject small pulses of liquid for the electrospray. The spray is accelerated into the trap via the high voltage gradient. The selection of trapping fields and needle potential are correlated to yield effective and efficient trapping of the charged particles. Utilizing a specific

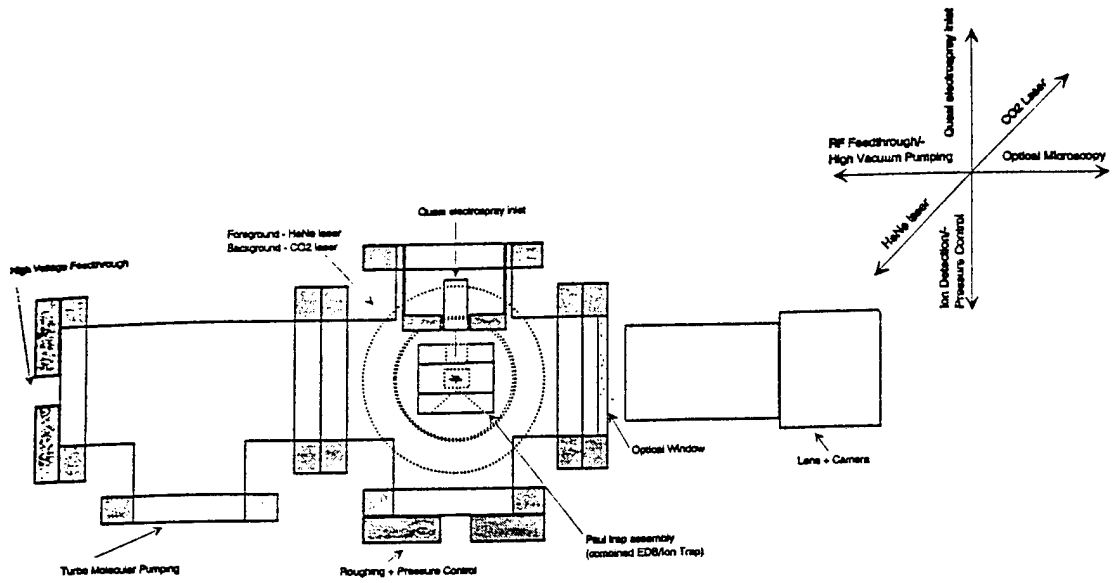

Figure 2. Particle levitation apparatus.

needle size, geometry and solvent, the voltage is adjusted to give a desired initial droplet size[6] which is slightly larger than the particle size (so that the mass does not decrease much during evaporation). The charge level is slightly below the Rayleigh limit using a 2.2 KV needle voltage. This allows nearly 10^6 charges on a 10μm particle.

This is an extremely high charge to mass ratio (~10^{-8} charges per Da) which gives these particles a high immunity to destabilization by air drafts within the system. This allows the system, at relatively low trapping voltages (<100 V rms), to be pumped from atmosphere to 10^{-3} torr in less than 5 min.

Using the 2.2 KV needle voltage, droplets are initially trapped using a ring voltage of ~300 V p-p at 300 Hz. While the end cap DC voltage difference is ~1 V. As the solvent evaporates particles become visible near the center of the trap. The electrospray is performed at atmospheric pressure both because of fear of glow discharge and to utilize the high damping values to decellerate the charged particles entering the trap. Although the electrospray droplet is accelerated by large electric fields at the needle tip, the atmospheric damping yields a large number of trapped particles from a single pulse of liquid (a few μL).

Below 10^{-3} torr the frequency and voltage of the trap is increased up to about 1 KHz and 1000 V p-p in order to avoid Mathieu instability of the particle since the effects of drag on the stability map are not seen at these pressures. Pressures below 10^{-7} have been obtained without destabilizing the particle.

RESULTS AND DISCUSSION

To trap a charged particle the following conditions should be met:

1) the trapping potential well should be deep enough in both r and z directions to stabilize the incoming particle. Typically the axial dimension is critical due to gravitational considerations. The particles will be trapped if

$$eU_z > |mgz_o - .877eV_{DC}|$$

and

$$U_z = \frac{eV_o^2}{4mz_o^2(\Omega^2+\Delta^2)}$$

where e is the charge on the particle, V_o is the RF amplitude, z_o is the axial dimension, Ω is the angular frequency and Δ is the damping time constant. Additionally U_z must be sufficiently large to accomodate additional particle perturbations due to electrical noise molecular collisions at low pressures and due to air currents at higher pressures.

2) On the other hand, the Q_z parameter of the particle may not exceed the Mathieu stability threshold.

$$Q_z = 2\frac{eV_o}{mz_o^2\Omega^2} = 2Q_r$$

This threshold for $\Delta=0$ is $Q_z=0.909$ and is increasing with the second power of the drag parameter $D=\Delta/\Omega$. Figure 3 illustrates the stability map for two values of the drag parameter.

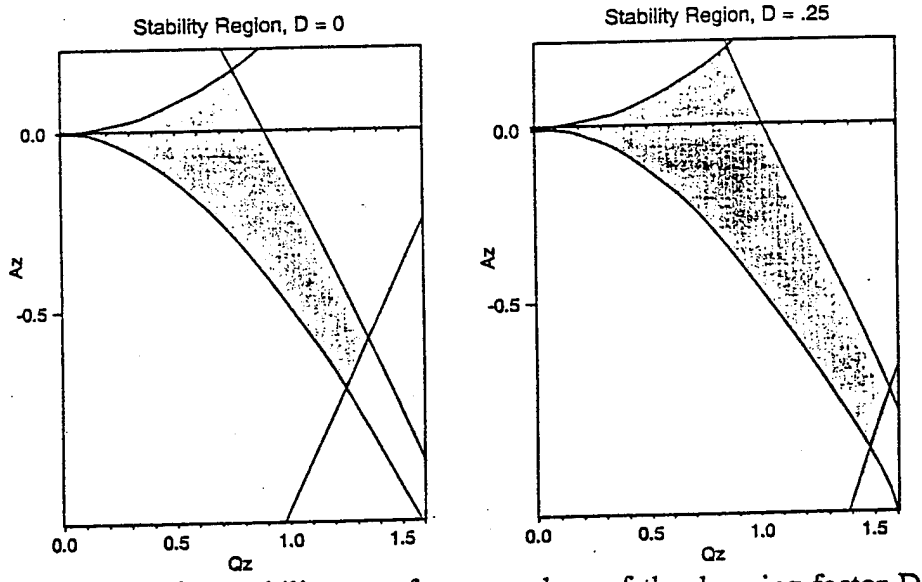

Figure 3. Mathieu equation stability map for two values of the damping factor D.

3) Sufficient damping of injected particles must be present in order to insure sufficient numbers of particles are trapped in the potential well. Figure 4 indicates the damping time constant as a function of particle size and pressure. When Δ is greater than the trapping frequency Ω, energy loss to drag is sufficiently rapid that high capture efficiencies may be expected.

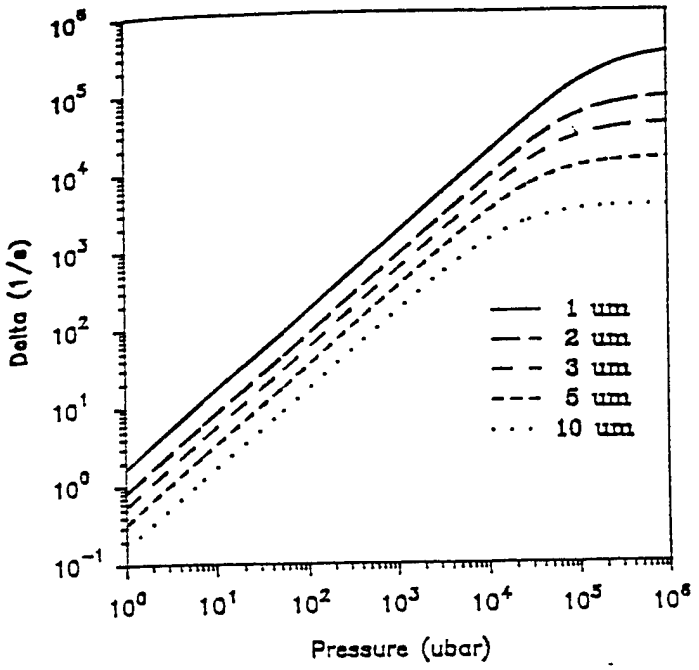

Figure 4. Particle damping factor as a function of gas pressure. Computed for air at 20 C.

These three conditions yield competing criteria for particle stability. Large damping time constants are required to decellerate the electrosprayed particles, but they lead to low trapping potentials so particles are easily destabilized. Large voltages and low frequencies yield deep potential wells, but may lead to particle instability. Ultimately one selects a compromise to best accomodate a particular m/z value being produced by the electrospray. Clearly the highest e/m ratio give the greatest degree of particle control. During sample introduction, several particles may be trapped. The trapping voltages and frequencies are manipulated to obtain a single particle in the trap. It should be noted that while multiple particles may be simultaneously stabilized, electrostatic repulsion between them prevents either particle being damped to the null point of the trap.

After stabilizing a single particle, pump down is made gradually. In the hundred torr range, speeds up to about 2 torr/sec pressure reduction will not to blow out the particle. At about 20 torr the trapping voltage should be lowered to 150 Vrms to avoid arcing. When the pressure goes to 10^{-3} torr range, the frequency of the drive is increased to avoid Mathieu instability, while the trapping voltage is also increased to about 600 Vrms to maintain sufficient trapping potential.

Figure 5 illustrates a single bacillus subtillus cell (~3 μm is diameter) suspended at 10^{-7} torr. The particle trajectory forms a Lysijou figure due to the superposition of different axial and radial oscillation frequencies. The amplitude is approximately 100 μm across.

Figure 6 illustrates the same particle at 10^{-7} immediately (< 5s) after pressuring the chamber to 10^{-3} torr and pumping to back out. The trajectory of Figure 4 will be fully developed after a number of minutes. In this case, the particle has been mechanically excited by vibrating the electrode assembly. The particle location is localized within 50 μm, which is adequate for precise laser targeting.

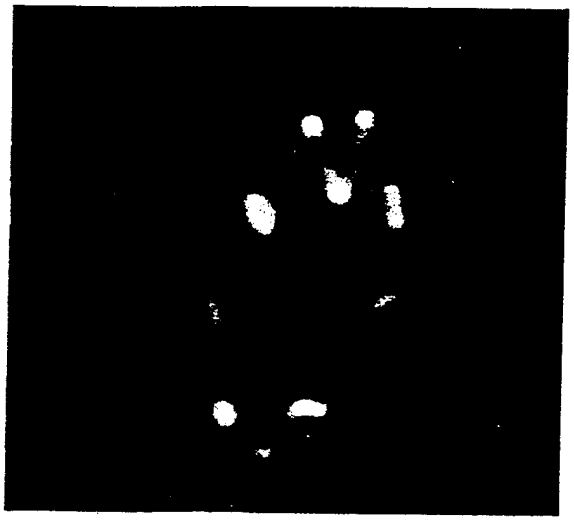

Figure 5. Bacillus subtillus cell suspended at 10-7 torr. Image particle motion over 1 video frame (1/30 s).

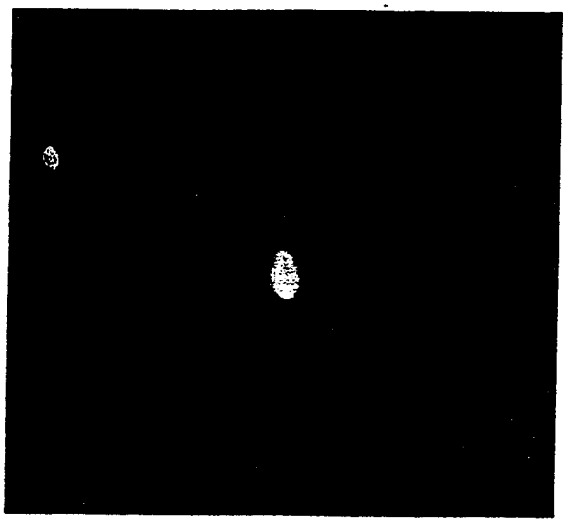

Figure 6. Same particle as Figure 5, immediately after application of damping gas.

REMAINING CHALLENGES

Laser Pyrolysis/Desorption/Ionization

A pulsed TEA CO_2 laser will be used with dual pulse time option (10 ms and 200 ms) and capable of producing 300 mJ pulses in TEM_{00} mode. Previous work with in-source CO_2 laser pyrolysis of biological samples has conclusively established the occurrence of quasimolecular ion formation, particularly cationized species, of relatively large biomolecules due to laser desorption/ionization processes[4].

Mass Spectrometric Detection of Product Ions

This task utilizes additional high frequency, ion trap type mass scanning electronics and wil require that EDB electronics be shut off in <10 ms prior to the laser pulse to prevent destabilization of resulting ions. Considerable optimization to obtain sufficient ion yield without excessive space charge will be required.

Detection and Identification of Biological Aerosol Particles

The complexity of biological materials require subsequent analysis which will focus on several areas: (1) the usage of pattern recognition and multivariate data analysis methods to extract "finger prints" of various biological materials. (2) The usage of MS/MS techniques to distinguish the origin of various ions which may be associated with particular materials. (3) The expansion of the mass range to higher m/z values to enable examination of particular molecular ions which in themselves may be more highly characteristic of various biological samples.

CONCLUSIONS

It is believed that 10^{-3} torr will be a sufficiently low system pressure to perform the laser pyrolysis and mass spectrometry on a particle. If lower pressures are required, stabilization of various particles, including 13 μm paper mulberry pollen, latex microspheres below .93 μm and bacillus subtillus organisms and spores, have been obtained at pressures down to 10^{-7} torr, but achieving these pressures may require special measures to contain the size of the particle trajectory and to remove condensate (primarily H_2O) in the vacuum system that limits pumpdown speed below 10^{-3} torr.

The expansion of particle trajectories below 10^{-3} torr is due primarily to thermal and electrical noise which is no longer damped out by the gas damping forces. In this region the "Matthieu" trajectories are readily observed (see Figure 5). It is not clear if these trajectories may be damped by electrical means, but initial efforts indicated that if damped by pressures on the order of 10^{-3} torr, the particle can be stabilized back at the center of the trap. Expansion of the trajectory after the pressure is back to 10^{-7} may take several minutes, so that gas leaks provide an effective stabilization compatible with high vacuum pyrolysis experiments.

It was anticipated that the position would be less localized at reduced pressure and that additional means would be necessary to maintain the particle at the trap center for laser targeting. It was not anticipated that it would be so stable to such a low pressure. The ability to trap particles under these conditions has provided a new opportunity to study "ion trajectories" as a function of pressure and trapping conditions. Pursuit of this area could provide valuable insights into resolution enhancements provided by resonance ejection[7] and into the process of collision induced dissociation in Ion Trap MS instruments.

Finally, it was not anticipated that the visibility of submicron particles will be so good. This is mainly due to the high sensitivity of the CCD camera for the wavelength of HeNe laser emission (632 nm).

ACKNOWLEDGEMENTS

The authors wish to thank Dr. J.P. Dworzanski for biological sample preparation. This research was supported by the Army Research Office under grant #DAAL03-91-G-0296.

REFERENCES

1. Davis, E.J. *Langmuir*, 1, **1985**, 379-387.
2. Kaiser, R.E. Jr.; Cooks, R.G.; Mass, J.; Heinburger, P.H. *Rapid Commun. Mass Spectrom.*, 3, **1989**, 50.
3. Kaiser, R.E.; Lowis, J.N.; Army, J.W.; Cooks, R.G. *Rapid Commun. Mass Spectrom.*, 3, **1989**, 225.
4. Posthumus, M.A.; Kistemaker, P.G.; Meuzelaar, H.L.C.; Ten Noever de Brauw, M.C. *Anal. Chem.*, **1978**, 50, 985-991.
5. Maswadeh, W.; Roberts, K.A.; McClennen, W.H.; Meuzelaar, H.L.C.; Arnold, N.S. *Proc. 37th ASMS Conf. on Mass Spec. and All. Topics*, Miami Beach, FL, **1989**.
6. Smith, D.P.H., *IEEE Transactions on Industry Applications*, **1986** 1A-22, 3, 527.
7. Goeringer, D.E.; Whitten, W.B; Ramsey, J.M.; McLuckey, S.A.; Glish, G.L.; *Anal. Chem*, **1992**, 64, 1434.

Mass Determination of Trapped Micro-particles and Macro-ions by Optical Techniques (and Subsequent Chemical Analysis by Laser Pyrolysis Mass Spectrometry)

Gyorgy Hars*, Neil S. Arnold and Henk L.C. Meuzelaar
Center for Micro Analysis & Reaction Chemistry
University of Utah, Salt Lake City, UT 84112

* Visiting scientist from TU Budapest, Hungary

Extensive analytical interest in characterization of particulate matter extends in many applications to evalution of individual micro-particles. For complete chemical characterization of individual microparticles adequate measurements of both particle physical characteristics (e.g., size, mass) and chemical constituents are required. Like molecular species, particles may also be readily ionized and manipulated by electrical techniques based on mass to charge ratios. An approach favored by the authors would provide an accurate mass determination which could be followed by laser pyrolysis (ionization) mass spectrometry to determine the chemical composition. Both measurements can be carried out in the same ion trap but they require different electrical operating conditions. For particle mass determination the ion trap operates as an Electrodynamic Balance (EDB) [1] while the compositional analysis is performed in the Ion Trap Mass Spectrometer (ITMS) mode. Figure 1 shows the typical operating parameters for both of the two modes. For macro-ions and submicron particles the distinction between ions and charged particles may become blurred making it profitable to consider the ability to make mass measurements of individual submicroparticles based on optical detection techniques.

The present investigation utilized the apparatus illustrated in Figure 2. A 10 mW HeNe laser illuminates the particle through a 3 mm hole in the ring electrode. A high sensitivity CCD camera with a zoom lens detects 90° scattered light via a second hole in the ring or via a hole in the end cap. Particles are introduced from suspension in water or alcohol by syringe needle inserted through the end cap. Strong electric fields used for trapping provide particle charging in a "quasi electrospray" ionization manner.

In classical EDB operation, gravitational force is offset by a DC potential applied in a dipolar mode to the two end caps making it possible to calculate the mass to charge ratio from the DC voltage applied. To obtain an accurate measurement the particle is damped to a small trajectory at the center of the trap and the end cap voltage measured (see Figure 3). Such measurements have been made to a relative accuracy of 1 in 10^5 [2]. In ITMS mode, secular oscillations of various ions are used to selectively eject ions. These same oscillations could be used to detect macro-ions, but the rapid motion (>100 Hz) and poor light scattering tend to make optical detection impractical. One means to overcome this limitation is to excite "standing" patterns reinforced by repetition of the same trajectory. This is not readily obtained in the r-z plane, but if viewed through an endcap the particle is seen to traverse an elliptical "Lissajous" pattern in the x-y plane. Superimposed on this pattern are drive frequency oscillations forming a "star" pattern as in Figures 4 and 5. This pattern will rotate unless the trapping frequency is an exact integer multiple of the radial secular frequency. By measuring the precession rate the secular frequency is determined allowing the m/z value to be calculated. At present the resolution is limited by a "beating" of 2 radial secular frequencies causing the "star" to collapse to a line every 3-10 seconds. In spite of this limitation current m/z measurements can be made to 1 part in 10^3. Finally, actual mass measurements (rather than m/z measurements) may also be utilizing single electron loss events induced by UV radiation. In principle, therefore it is possible to determine the mass of a single macro-ion in the 10^9-10^{12} a.m.u. range with similar precision. Calculations suggest the possibility of extending this approach to particles in the 10^1-10^2 nanometer range (10^6-10^9 a.m.u.), thus indicating the feasibility of developing a novel optical method for high precision mass determination of a single macro-ion.

Acknowledgements

This work was sponsored by the U.S. Army Research Office (Grant #DAAL03-91-G-0296). The authors would like to acknowledge helpful discussions with Drs. Randy Long (ARO) and Asit Ray (University of Kentucky).

References

1. Davis, E.J. and Ray, A.K., *J. Colloid Interface Sci.* 75, 2 (1980) 566.
2. Philip, M.A., Gelbard, F., Arnold, S. *J. Colloid Interface Sci.* 91,2 (1983) 507.

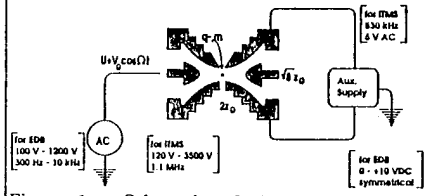

Figure 1. Schematic of the EDB/ITMS arrangement. The operating conditions are displayed in parentheses.

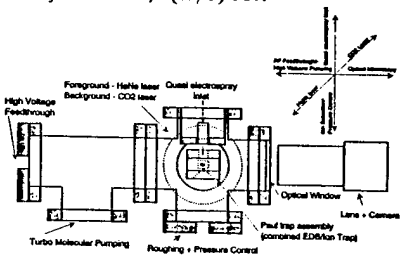

Figure 2. Physical layout of the experimental setup. The direction of optical observation of the particle is normal to the illuminating HeNe beam. The pyrolyzing carbon dioxide laser beam is parallel to the HeNe laser beam. The ions created by the pyrolysis are emitted in vertical z direction.

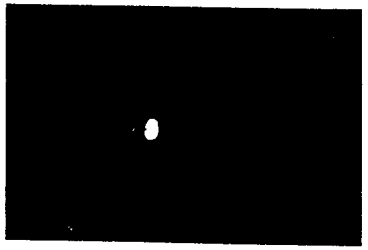

Figure 3. The effect of 10^{-4} torr He buffer gas. The particle is standing still in the center of the trap during the EDB measurement.

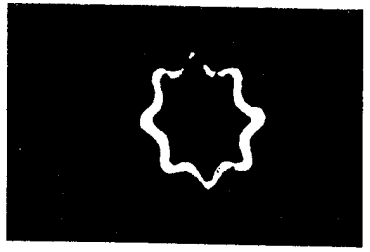

Figure 4. Eight point star pattern of a 1 micron particle in the equatorial plane of the ion trap.

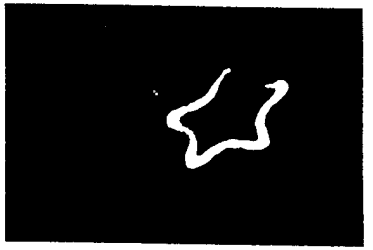

Figure 5. Five point star pattern of a 1 micron particle in the equatorial plane of the ion trap.

Abstract:

From the Abstract Book for the American Chemical Society Meeting, Chicago, IL, August 1993.

CHEMICAL CHARACTERIZATION OF SINGLE AEROSOL PARTICLES VIA COMBINED ELECTRODYNAMIC BALANCE/ION TRAP MASS SPECTROMETRY TECHNIQUES. Neil S. Arnold, George Hars and Henk L.C. Meuzelaar; Center for Micro Analysis and Reaction Chemistry, University of Utah, Salt Lake City, UT 84112.

The electrodynamic balance (EDB) has been used for various studies of individual aerosol particles with respect to a variety of physical and optical properties. Ion Trap mass spectrometry requires the same electrode configuration although different operating voltages are used. The use of combined EDB and Ion Trap techniques for chemical evaluation of single aerosol particles allows initial particle evaluation with respect to size and weight to be obtained via optical techniques during initial particle suspension, while laser pyrolysis/desorption is used to generate ionic species which are mass analyzed for chemical characterization of the particle via Ion Trap mass spectrometry. Optical detection and stabilization of individual aerosol particles may be performed for particles less than 1 micron to over 100 microns in diameter. Novel methods for determining the mass of these particles prior to laser pyrolysis/desorption will be described as well preliminary mass spectrometric evaluation of the products used for particle characterization.

EDGEWOOD
RESEARCH, DEVELOPMENT & ENGINEERING CENTER
U.S. ARMY CHEMICAL AND BIOLOGICAL DEFENSE COMMAND

ERDEC-SP-024

PROCEEDINGS OF THE 1993 ERDEC SCIENTIFIC CONFERENCE ON CHEMICAL DEFENSE RESEARCH 16-19 NOVEMBER 1993

Dorothy A. Berg
Joseph D. Williams, Jr.
Patricia J. Reeves

RESEARCH AND TECHNOLOGY DIRECTORATE

August 1994

Aberdeen Proving Ground, MD 21010-5423

CHEMICAL CHARACTERIZATION OF SINGLE AEROSOL PARTICLES VIA COMBINED ELECTRODYNAMIC BALANCE/ION TRAP MASS SPECTROMETRY TECHNIQUES

Gyorgy Hars*, Neil S. Arnold and Henk L.C. Meuzelaar

Center for Micro Analysis & Reaction Chemistry
University of Utah, Salt Lake City, UT 84112

*Technical University of Budapest,
Dept. Atomic Physics 1111 Budapest Budafoki str.8 Hungary

ABSTRACT

A multifunction Paul trap is described capable of trapping, stabilizing and analyzing electrostatically charged microparticles as well as a broad range of ions and macro-ions. Typically, particles in the 0.1-10 μm range are introduced by aerosolization from an aqueous suspension, although quasi-electrospray and dry powder type introduction methods can also be used. A new particle trajectory pattern, observed in the equatorial plane, was found to offer a nondestructive, optical method for determining the m/z value of microparticles and macro-ions, with a present accuracy of $1:10^3$ and a potential maximum resolution of $1:10^6$. Recent addition of a more powerful laser (Nd YAG, operating at 1.06 μm) has enabled us to generate laser fragmentation/ionization mass spectra of 1 μm dia polystyrene particles and of *Bacillus subtilis* spores. Current shot-to-shot reproducibility is still unsatisfactory and some as yet unresolved, mass calibration problems have been encountered. Nonetheless, the high intensity and apparent complex organic nature of the ion signals obtained might herald the emergence of a novel MS technique for chemical and physical characterization of single microorganisms and other components of respirable aerosols.

INTRODUCTION

The development of a multifunction (electrodynamic balance + ion trap mass spectrometer) Paul trap capable of trapping, stabilizing and analyzing microparticles (ranging in size from 0.1 to several tens of microns) as well as ions (ranging in size from a few Daltons to gigaDaltons) was undertaken for the primary purpose of obtaining characteristic mass spectra of single microorganisms and other respirable aerosol particles. As reported at the 1992 ERDEC Scientific Conference[1] successful trapping and visualization of micron-, or even

submicron-, sized particles injected by means of various aerosolization methods was accomplished in a modified Finnigan MAT type ion trap electrode assembly. Optimization of the trapping potential, using a square wave drive frequency, was shown to enable evacuation of the chamber to less than 10^{-4} torr without destabilizing the trapped particle. However, preliminary attempts to produce characteristic mass spectra by means of hitting the stabilized particle with the focussed beam of a small TEA CO_2 laser failed to produce adequate ion signal. Serendipitously, particles trapped at pressures $<10^{-4}$ torr were observed to exhibit a previously unreported star-shaped trajectory in the equatorial plane. This trajectory was found to be a function of m/z value.

The present report describes the evolution of a novel, nondestructive optical method for determining the mass of a single megadalton ion (or microparticle) with a potentially high degree of accuracy. Secondly, the authors report the installation of a more powerful (Nd, YAG type) laser and the results of preliminary laser fragmentation/ionization (LFI) MS studies on polystyrene microparticles and *Bacillus subtilis* spores.

EXPERIMENTAL

Instrumentation

Figure 1 shows the experimental setup. A modified Finnigan ITD 700 ion trap electrode assembly is used. The ring electrode has three radial drill holes (3 mm dia). Two are directly in line with each other, the third one is positioned at a 90 degree angle. The two aligned holes carry the HeNe laser beam through the center of the trap. The perpendicular hole is used to detect and observe particles in the center of the trap levitated by means of a long working distance optical microscope (Cohu 312985) with highly sensitive CCD camera (Cohu 6410). The camera can also be operated from a vertical position for observing the center of the trap through the central hole in the upper end cap. The ring electrode is driven with a rectangular voltage signal ranging from 500 Hz to 3 kHz in frequency and up to 2 kV in amplitude. The end cap electrodes are driven by a power supply providing both DC and/or AC modulation in common or in opposite phase mode. A UV lamp placed underneath the trap projects its light through the central hole of the lower end cap, thus illuminating the center of the trap. The pulsed beam (5 ns, 450 mJ) of the Nd-YAG laser (Continuum, Surelite J-10) is focussed to the center of the ion trap without illuminating any part of the electrode system. The trap is contained within a UHV vacuum housing with suitable view ports. The necessary pumping is provided by a 170 l/s TPU 170 Balzers turbo pump+ rotary forepump combination. During evacuation of the trap, the pressure is monitored by means of a Baratron gauge.

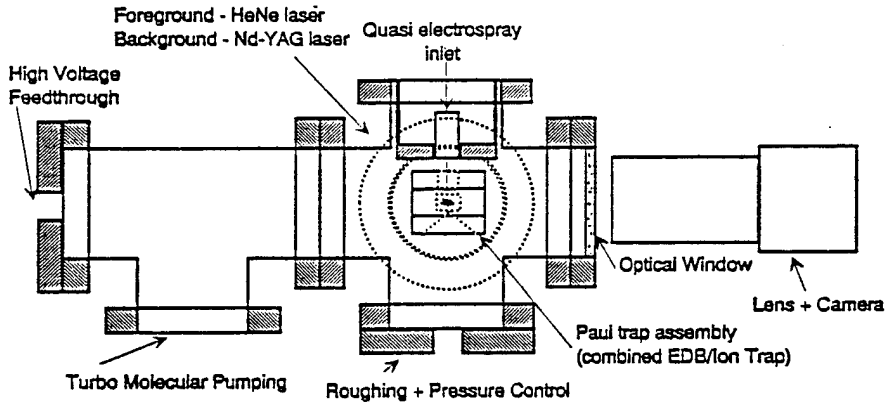

Figure 1. The experimental setup of the particle analyzer equipment.

Experimental Methods

First the particles are suspended in water and then introduced into the ion trap by means of a syringe through the central hole of the upper end cap. Because of the high electric field in the trap most of the particles will be spontaneously charged. The initial value for the mass/charge ratio is about 10^9 a.m.u./unit charge. Generally more than one particle is trapped. Particles near the center of the trap are being visualized by means of the HeNe target beam and a highly sensitive video microscopy system. Applying opposite mode DC on the end caps and gradually increasing the drive frequency of the ring results in ejecting all particles except one. This particle will be centered in the trap. Subsequently the vacuum system is gradually pumped down to $<10^{-4}$ torr. In order to avoid arcing in the trap during evacuation, a rectangular voltage signal is used to drive the ring electrode. The rectangular signal provides the highest possible trapping potential at limited (200 V) voltage amplitude at high drag conditions. Below 10^{-4} torr the particle reveals highly characteristic and stable oscillation patterns. In the equatorial plane of the ion trap the particle performs an elliptical motion. At specific voltages and frequencies the rapidly circulating particle can be observed as a quasi standing oscillation which resembles a star pattern (see Figures 2 and 3). By counting the "branches" of the star and measuring the corresponding voltage and frequency, the mass/charge ratio of the particle can be calculated. Subsequent UV radiation to induce stepwise electron loss events enables the absolute mass of a single macro-ion in the 10^9-10^{12} Dalton range to be determined.

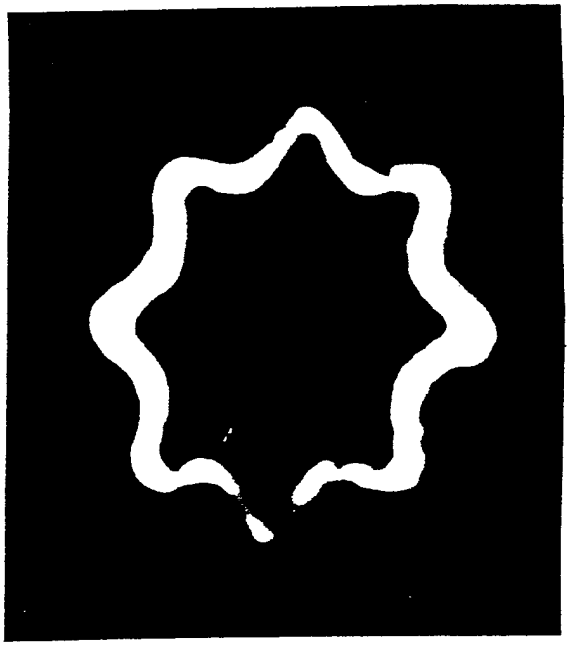

Figure 2. Eight branch star pattern of a 1.0 μm diameter polystyrene particle to the equatorial plane of the ion trap.

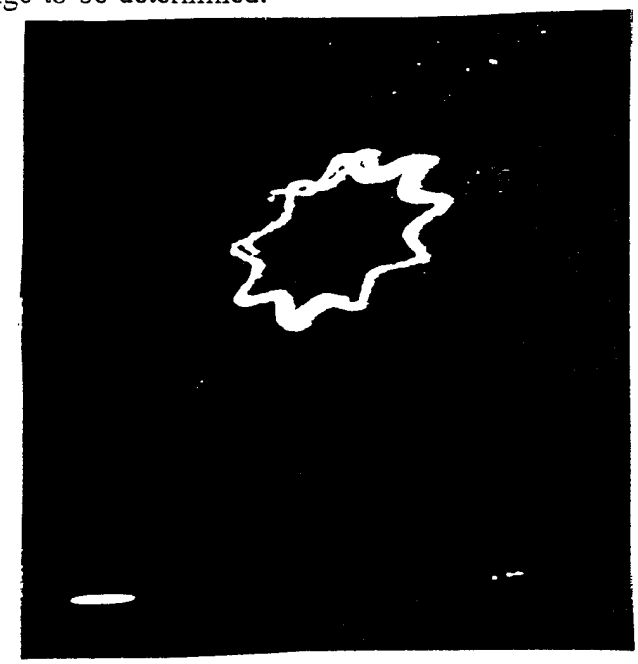

Figure 3. Nine branch star pattern of a 1.0 μm diameter *B. subtilis spore* particle in the equatorial plane of the ion trap.

Chemical characterization is performed in the same Paul trap, while operating in the Ion Trap Mass Spectrometer (ITMS) mode. Moreover, since the mass determination procedure is nondestructive, the same microparticle or macro-ion can be analyzed while still stabilized in the

trap. First He buffer gas is introduced into the vacuum system to 10^{-4} torr. Because of the increased drag, the star pattern of the particle shrinks until the particle appears as a single bright dot in the center of the trap. Subsequently, the trapped particle is fragmented and ionized by means of a single, 5 ns, 450 mJ pulse from a Nd YAG laser operating at 1.06 μm. Simultaneous with the laser pulse the electronic drive of the ring electrode is switched from the mass determination to the ITMS mode in order to record a mass spectrum of the ion fragments created by the laser shot (Figures 4 and 5).

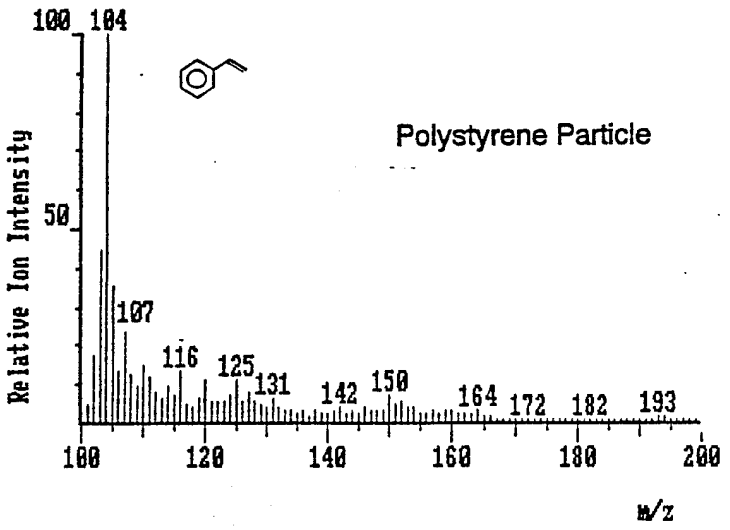

Figure 4. LFI mass spectrum of a 1 μm dia. polystyrene particle (or a small cluster of particles) showing dominant ion peak at m/z 104, believed to represent the styrene monomer unit. The pattern shown is not very reproducible in that repeat shots may show a similar ion cluster at m/z values anywhere between m/z 104 and 110.

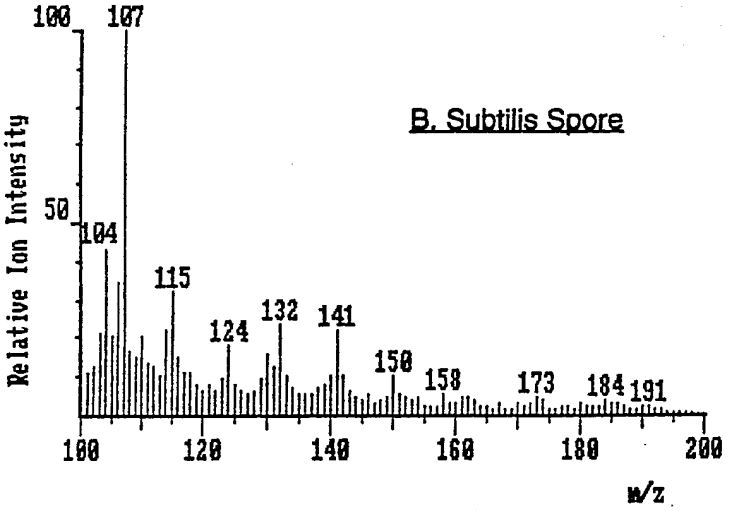

Figure 5. LFI mass spectrum of a *Bacillus subtilis* (or a small cluster of several spores) showing a more complex pattern than Figure 3. A similar type of pattern was found in about 40-50% of the *B. subtilis spore* analyses. Note frequent peak intervals of 15, 17, 18 and 26 amu, suggesting dominant organic ion signals.

RESULTS AND DISCUSSION

Mass Determination of the Particle

A theoretical discussion of the novel mass determination principle introduced here is based on the pseudo-potential model of the ion trap[2]. In this model the charged particle is considered to be in a spring-like linear force field, although the spring constants D_r and D_z are unequal. For mathematical purposes the origin of a Cartesian coordinate system is put into the center of the trap. The x and y axis are in the equatorial plane and the electrode system is rotationally symmetric around the vertical z axis. Since x and y are equivalent they will be

often referred as r (standing for radial direction). The vector of average force affecting the charged particle is F.

$$F = -D_r(xi+yj) - D_z zk \qquad (1)$$

Here i, j, k are the unit vectors of the coordinate system in x, y and z directions respectively. The values of D_r and D_z are derivable from the model and are as follows:

$$D_r = \frac{1}{2m}\left(\frac{QV}{r_o^2\Omega}\right) \qquad D_z = \frac{2}{m}\left(\frac{QV}{r_o^2\Omega}\right)^2 \qquad (2)$$

where D_r and D_z are the spring constants, m and Q are the mass and charge of the particle, V and Ω are the voltage amplitude and the angular frequency of the drive and finally r_o is the radius of the ring electrode.

Apparently, the "spring" in z direction is four times stronger than in r direction. ($D_z = 4D_r$) The equation of motion can readily be solved. The x and y components are identical. The motion in each direction is a harmonic oscillation. The oscillation frequency in x,y and z directions are $\omega_x=\omega_y=\omega_r$ and ω_z respectively:

$$\omega_r=\sqrt{\frac{D_r}{m}} \qquad \omega_z=\sqrt{\frac{D_z}{m}} \qquad (3)$$

These are the so-called secular frequencies. Obviously the secular frequency in z direction is twice higher. Substituting (2) into (3) the values of the secular frequencies result as:

$$\omega_r=\frac{\sqrt{2}}{2}\frac{QV}{m\,r_o^2\Omega} \qquad \omega_z=\sqrt{2}\frac{QV}{m\,r_o^2\Omega} \qquad (4)$$

So far the average force affecting the particle was considered to be a function of position only. In reality this average force is the result of several "pushes and pulls" so the trajectory of the particle shows a fine structure which is synchronous with the drive frequency. If the drive frequency/secular frequency ratio is an integer then the fine structure on the trajectory will seem to be standing. In the case of the elliptical motion in the equatorial plane the fine structure due to drive frequency will result in a standing star pattern provided that the star pattern condition is met:

$$n\,\omega_r = \Omega \qquad (5)$$

where n is an integer. From (5) the mass/charge ratio of the particle can readily be expressed: The value of n can be obtained by counting the branches of the star. By means of (6) the mass/charge ratio can be determined by adjusting a standing (mostly eight branch) star pattern

$$\frac{m}{Q} = \frac{\sqrt{2}}{2} \frac{n\,V}{r_o^2\,\Omega^2} \qquad (6)$$

and by measuring the voltage and the frequency of the corresponding drive.

Illuminating the negatively charged particle with very faint UV light the electrons will be removed from the particle one by one[3]. Some second succession can be readily adjusted by using faint enough UV light. If the particle to be analyzed is in a standing star pattern the loss of electrons will cause the pattern to spin again. Then the pattern can be stabilized by reducing the drive frequency. The mass/charge ratios before and after the electron loss can be expressed by means of (6):

$$\frac{m}{Z\,e} = \frac{\sqrt{2}}{2} \frac{n\,V}{r_o^2\,\Omega_1^2} \qquad \frac{m}{(Z-1)e} = \frac{\sqrt{2}}{2} \frac{nV}{r_o^2\,\Omega_2^2} \qquad (7)$$

where Z is the ionization level, e is the elemental charge 1.6×10^{-19} as, Ω_1 and Ω_2 are neighbor drive frequencies. The absolute mass can be calculated from (7):

$$m = \frac{\sqrt{2}}{2} \frac{n\,V\,e}{r_o^2\,(\Omega_1^2 - \Omega_2^2)} \qquad (8)$$

Since the particle carrier at least several hundred unit charges the measurement can be repeated a number of times, thus making the method more dependable.

Laser Fragmentation/Ionization MS

The LFI mass spectrum of a 1.0 μm polystyrene particle illustrated in Figure 4 is characterized by the occurrence of mass peaks at every nominal m/z value within the selected mass range. Furthermore, the mass intensities are quite high (typically 10^5-10^6 "ion counts" full scale). Finally, the spectrum appears to be dominated by organic compound signals in view of the frequent occurrence of 14, 15 or 28 amu intervals rather than the m/z 23 or 39 intervals characteristic of sodium and potassium ion contributions or the 12 amu intervals associated with carbon cluster formation. Unfortunately, detailed chemical interpretation of the mass spectrum in Figure 3 is presently impossible since the signals do not directly correspond to the expected styrene and styrene-like decomposition products. The most likely explanation is that the high initial concentrations of ions in the ion trap are causing significant shifts in the mass scale calibration. Similarly, the *B. subtilis* spore spectrum in Figure 5 also provides high ion intensities combined with a current lack of biochemical interpretability. Complex secondary reactions, e.g., due to excessive laser intensities and/or an unknown mass scale calibration shifts due to space charge phenomena in the trap may well be responsible for these problems. Before any detailed conclusions can be drawn, however, it will be necessary to confirm the organic nature and information content of the ion signals observed. Since the ion trap system can be

operated in a tandem MS mode it should be possible to produce daughter ion spectra and thus identify some of the major peak signals in Figures 4 and 5.

CONCLUSIONS AND RECOMMENDATIONS

Conclusions:

1) Micron- and submicron-sized particles can be trapped from electrospray sources from vaporized suspensions in H_2O, or directly from air.
2) Trapped particles can be pumped down to high vacuum ($<10^{-4}$ torr) conditions without loss of stability.
3) Under high vacuum conditions particles describe a star like pattern in the equatorial plane that can be used for precise mass/charge ratio determinations.
4) Use of a Nd YAG laser beam at 1.06 μm produces intense ion signals from single styrene particles or *B. subtilis* spores which appear to represent complex organic compounds.

Recommendations:

1) Further experiments are needed to optimize Nd YAG laser pulse intensities beam alignment and choice of wavelengths (the 1.06 μm wavelength can be doubled, tripled or quadrupled), especially in order to increase shot-to-shot reproducibility.
2) Use of tandem MS techniques should enable identification of the presently unknown ion signals.
3) A systematic of different types of aerosol particles, supported by pattern recognition methods will be needed to evaluate the practicality of the LFI-MS technique.

ACKNOWLEDGEMENTS

The authors want to acknowledge helpful advice from Randy Long and Robert McLane, as well as the expert technical assistance of Paul Cole. This work is being funded by the U.S. Army Research Office (contract #DAAL03-91-G-0296).

REFERENCES

1. Arnold, N.S.; Hars, G.; Cole, P.A.; Meuzelaar, H.L.C., Proc. 1992 US Army ERDEC Scientific Conference, 1993, 219.
2. Wuerker,R.F.; Shelton,H.; Langmuir,R.V. J.Appl.Phys. 30(3), 1959, 342.
3. Arnold, S.J., Aerosol Sci., 10, 1979, 49.

Extended Theoretical Considerations for Mass Resolution in the Resonance Ejection Mode of Quadrupole Ion Trap Mass Spectrometry

Neil S. Arnold, György Hars,* and Henk L. C. Meuzelaar
Center for Micro Analysis and Reaction Chemistry, University of Utah, Salt Lake City, Utah, USA

Proceeding from the pseudopotential-well approximation for ion motion in a quadrupole ion trap, mathematical expressions are derived to describe the excitation amplitude of an ion packet at a given mass-to-charge ratio. Ion-neutral collisions are incorporated to describe the damping of ion trajectories and to describe the distribution of individual ion trajectories about a mean amplitude for the ion packet. The rate of increase of the amplitude during scanning is related to expressions that describe the amplitude dispersion of the ions at the time of ejection from the trap, which is operating in a resonance ejection scanning mode to describe the temporal line width of the ejected ion packet. The temporal line width is related to mass resolution under a number of different scanning conditions. Included in the discussion are considerations of the effect on resolution of the resonance excitation voltage, temperature, pressure, noise, and buffer-gas composition. An expression for the maximum possible resolution at high ion mass-to-charge ratios is developed, and these results are compared to an existing theoretical construction. The expressions derived under the pseudopotential-well approximation are further extended to high q_z values and compared to experimental data previously published by two other researchers. *(J Am Soc Mass Spectrom 1994, 5, 676–688)*

Recent work on high mass, high resolution ion trap mass spectrometry has shown that three-dimensional Paul-type [1] quadrupole instruments are capable of resolution exceeding one million [2, 3] and detection of ions with mass-to-charge ratios greater than 50,000 [4] during operation in the resonance ejection mode [5]. Although the theory that describes the mass scanning properties of ion-trap-type instruments in both the mass-selective instability mode [6, 7] and in the resonance ejection modes [8] is well established, even in systems incorporating nonlinear hexapole and octapole fields [9], theory that describes the resolution characteristics for the purpose of further optimization of instrument performance has been slow to develop.

In a recent article, Goeringer et al. [10] proposed a theoretical basis for understanding high resolution mass spectra obtained in quadrupole ion traps via resonance ejection. This theory is based on two fundamental assumptions. The first assumption requires that a pseudopotential-well description of ion motion, which was extended to include ion–molecule collisions, allows the amplitude excitations of the ion to be described by the response of a damped harmonic oscillator to an external driving frequency. The basis of this assumption is the work of Major and Dehmelt [11].

By using this assumption, the authors derived the amplitude response of an ion in the case of a linearly scanned excitation frequency. This response showed a clear dependence on scan rate and ion damping, and the width of this response line in frequency space was subsequently related to a mass line width to determine the mass resolution. The use of this frequency line width for ion excitations implies a second assumption. This assumption is that frequency dispersion of the amplitude excitation is equivalent (or at least proportional) to the spatial dispersion of the ion packet at ejection. In effect, this assumption implies that ions of a given resonant frequency are being ejected from the trap during the entire time that the excitation amplitude of the ion packet is nonzero, so that the temporal line width is the same as if the ions were not ejected at all.

In addition to not directly addressing the physics of ion packet ejection, this second assumption is troubling because it does not allow for a description of the effect of excitation amplitude on mass resolution. Furthermore, it is well known that a classical externally driven damped harmonic oscillator has no implied amplitude dispersion [12] beyond that implied by transient excitations and phase-angle differences. If scanned

Address reprint requests to Dr. Neil S. Arnold, Center for Micro Analysis and Reaction Chemistry, The University of Utah, EMRL, Building 61, Room 214, Salt Lake City, UT 84112.
*On leave from the Department of Atomic Physics, Technical University of Budapest, Budapest, Hungary.

1044-0305/94/$7.00

Received November 29, 1993
Revised February 10, 1994
Accepted February 10, 1994

sufficiently slowly and without any other amplitude dispersion mechanism, a damped harmonic oscillator with a fixed ejection amplitude should be capable of infinite resolution.

Figure 1 clarifies this point. The wide distribution in Figure 1 describes the ion packet oscillation amplitude as a function of time, assuming the behavior of a damped harmonic oscillator. The inset distribution near the z_0 axis represents an actual distribution of ion oscillation amplitudes around the mean at the moment of ion packet ejection. In a first-order approximation, the actual temporal line width at ejection (inset near the $a\tau t$ axis) is governed by the amplitude dispersion of the ion trajectories and the rate of amplitude increase. This line width may be considerably thinner than the temporal line width of the amplitude excitation of ions that are not ejected from the trap. In fact, if this amplitude dispersion approaches zero, the temporal line will also approach zero, corresponding to infinite resolution.

Furthermore, this second assumption is unnecessary because the same mathematical development of ion-neutral momentum transfer processes used to describe the collisional damping of ion trajectories also can be used to describe the amplitude dispersion of the ion packet at the point of ejection [13]. The amplitude dispersion of the packet then may be related to the rate of increase in the ion packet oscillation amplitude at ejection to obtain temporal and mass resolution line widths. These line width expressions yield resolution descriptions that may be compared to the resolution expressions obtained from the previous frequency line width assumption and to various experimental measurements.

Theory

As illustrated in Figure 1, the temporal line width of a group of ions ejected at a given mass-to-charge ratio

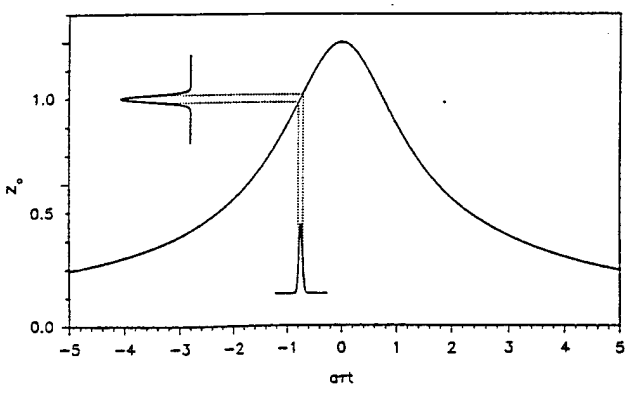

Figure 1. The relationship between ion packet excitation (full width curve), amplitude dispersion of the ion packet (inset left), and the actual temporal line width of the mass peak represented by the ion packet (inset center).

may be approximated by the expression

$$\Delta t = \frac{\Delta A}{dA/dt} \tag{1}$$

Here Δt is the temporal line width, ΔA is the amplitude dispersion at ejection, and dA/dt is the rate of increase of the ion packet amplitude at ejection. By using the pseudopotential-well approximation [7, 11], we compute dA/dt on the basis of considerations similar to those used by Goeringer et al. [10], whereas ΔA is derived from dispersion considerations in ion–molecule collisions.

Axial Excitation of Ion Motion

Ignoring the radial motion equations, we describe the axial motions as

$$\frac{d^2z}{dt^2} + c\frac{dz}{dt} + \omega^2 z = f_s \exp(i\omega_s t) \tag{2}$$

where

$$\omega = \frac{q_z \Omega}{2\sqrt{2}}$$

$$f_s = \frac{eV_s}{\sqrt{2}\, mr_o}$$

$$q_z = \frac{4eV}{mr_o^2\Omega^2}$$

The terms are defined as follows: z is the mean axial ion position, V is the fundamental rf drive voltage, e is the ion charge, m is the ion mass, r_o is the ring electrode radius, Ω is the fundamental angular drive frequency, V_s is the supplemental end cap excitation voltage, ω_s is the supplemental end cap excitation frequency, and c is the reduced collision frequency discussed below. The term ω_s is the secular frequency of unforced resonant oscillations, and f_s is amplitude of external forcing normalized per unit mass.

The substitution of $z = Z(t)\exp(i\omega_s t)$ into eq 2 along with an assumption that $Z(t)$ is a slowly varying function of time, $\omega \approx \omega_s$, and $\omega \gg c$ allows us to write

$$\frac{dZ}{dt} + \left(\frac{c}{2} + i\Delta_\omega\right)Z = \frac{-if_s}{2\omega} \tag{3}$$

where $\Delta\omega = \omega_s - \omega$.

It may be shown that if the secular frequency is swept linearly with time such that $\Delta\omega = at$, where a is the scan rate in radians per square second, then Z can be written as

$$Z(x) = \frac{-if_s}{2\omega\sqrt{a}} \exp\left(\frac{-x}{\sqrt{a}\,\tau} - \frac{ix^2}{2}\right) \times \int_{-\infty}^{x} \exp\left(\frac{\xi}{\sqrt{a}\,\tau} + \frac{i\xi^2}{2}\right) d\xi \tag{4}$$

where $x = a^{1/2}t$ and $\tau = 2/c$. The amplitude of the secular oscillation is determined by the absolute value of $Z(x)$, such that the amplitude $A = |Z(x)|$. To simplify subsequent operations, we define $F(x)$ as a dimensionless amplitude

$$F(x) = \frac{2\omega\sqrt{a}}{f_s}|Z(x)| = \frac{2\omega\sqrt{a}}{f_s}A(x) \tag{5}$$

where $F(x)$ is given by

$$F(x) = \exp\left(-\frac{x}{\sqrt{a}\,\tau}\right)\left[\left(\int_{\infty}^{x}\exp\left(\frac{\xi}{\sqrt{a}\,\tau}\right)\cos\left(\frac{\xi^2}{2}\right)d\xi\right)^2 + \left(\int_{\infty}^{x}\exp\left(\frac{\xi}{\sqrt{a}\,\tau}\right)\sin\left(\frac{\xi^2}{2}\right)d\xi\right)^2\right]^{1/2} \tag{6}$$

Direct evaluation of these integrals is difficult, and closed-form solutions do not exist, but as shown in refs 10 and 11, it is possible to utilize approximations for the two cases where $a^{1/2}\tau \gg 1$ and $a^{1/2}\tau \ll 1$. These integrals also may be evaluated numerically in regions where these simple approximations are not available.

For $a^{1/2}\tau \ll 1$, we utilize a result obtained by integration by parts, so that

$$F(x) = \frac{\sqrt{a}\,\tau}{\sqrt{1 + a\tau^2x^2}} \tag{7}$$

gives the excitation amplitude. This expression may be differentiated with respect to time to obtain

$$\frac{dF}{dx} = \frac{(\sqrt{a}\,\tau)^3x}{(1 + a\tau^2x^2)^{3/2}} \tag{8}$$

This latter equation describes the rate of increase of the ion envelope near ejection.

For the case of $a^{1/2}\tau \gg 1$ we require an approximation that describes the rising side of the amplitude envelope so that the slope in the vicinity of resonant frequency at $x = 0$ may be determined. In this limit, we can rewrite eq 6 in terms of Fresnel integrals [14], so that

$$F(x) = \sqrt{\pi}\sqrt{\left(\frac{1}{2} + C\left(\frac{x}{\sqrt{\pi}}\right)\right)^2 + \left(\frac{1}{2} + S\left(\frac{x}{\sqrt{\pi}}\right)\right)^2} \tag{9}$$

$$C(x) \equiv \int_0^x \cos\left(\frac{\pi\xi^2}{2}\right)d\xi$$

$$S(x) \equiv \int_0^x \sin\left(\frac{\pi\xi^2}{2}\right)d\xi$$

shows a square root dependence of the diffraction intensity pattern produced by an infinite straight edge in wave optics [15]. Subsequent differentiation with respect to x gives

$$\frac{dF}{dx} = \frac{\left(\frac{1}{2} + C\left(\frac{x}{\sqrt{\pi}}\right)\right)\cos\left(\frac{x^2}{2}\right) + \left(\frac{1}{2} + S\left(\frac{x}{\sqrt{\pi}}\right)\right)\sin\left(\frac{x^2}{2}\right)}{\sqrt{\left(\frac{1}{2} + C\left(\frac{x}{\sqrt{\pi}}\right)\right)^2 + \left(\frac{1}{2} + S\left(\frac{x}{\sqrt{\pi}}\right)\right)^2}} \tag{10}$$

Amplitude Dispersion

The average rate of momentum loss due to collisions is related to the reduced collision frequency c. A mathematical derivation for c is given by

$$c = \left(\frac{M}{m + M}\right)nv_r\sigma_D \tag{11}$$

where m is the ion mass, M is the mass of colliding neutrals, n is the number density of neutrals, v_r is the average relative speed of the colliding ion and neutral, and σ_D is the collision cross section, and proceeds from momentum transfer arguments that are outlined elsewhere [13], wherein the ion is assumed to be "drifting" in a constant electric field. The present developments assume that although the ions undergo accelerated motion in the ion trap oscillations, the average momentum damping is still the same.

The same arguments that allow the development of the reduced collision frequency expressions also may be applied to velocity dispersion of the ion packet [13] caused by collisions with neutrals. This dispersion is based on the discontinuous nature of the ion damping. Following Mason and McDaniel [13] and considering only the axial excitations of the ions, we write the relative velocity dispersion as for ions traveling at drift velocity v_d

$$(\Delta V_z)^2 = \overline{v_z^2} - v_d^2 = \frac{kT}{m} + \frac{C^*}{3}\frac{4m + M}{2m + M}\frac{M}{m}v_d^2 \tag{12}$$

where $(\Delta V_z)^2$ is the velocity dispersion about the mean v_d in the z direction, v_z^2 is the thermal average of the square of ion velocity in the z direction, k is the Boltzmann constant, T is absolute temperature, and C^* is a constant that has a value on the order of 1 depending on the m/M ratio and the nature of ion-neutral scattering.

As mentioned before, eqs 11 and 12 are both developed for the case of constant electric field. Use of eq 11 in the present case requires the assumption that the overall ion packet is in dynamic equilibrium with the

neutrals via collisions, so that c may represent the average damping of the ion packet. Equation 12 represents the fluctuations around this equilibrium, and the earlier assumption that $\omega \gg c$ implies that the velocity dispersion may be averaged over time by using the root mean square (rms) value of v_d. Further, because that particle is undergoing simple harmonic motion, the expression $v_z = \omega z$ allows us to relate the velocity dispersion to the amplitude dispersion of the ion packet.

The amplitude dispersion of the ion packet in dynamical equilibrium with the surrounding neutrals may therefore be represented as

$$\Delta A = \frac{1}{\omega_s}\sqrt{\frac{kT}{m} + \frac{C^*}{3}\frac{4m+M}{2m+M}\frac{M}{m}v_{rms}^2} \qquad (13)$$

where v_{rms} is the rms velocity amplitude due to the external driving field. At the point of ejection, $A_{ej} = r_o/2^{1/2}$, $v_{rms} = \omega_s r_o/2$ and substitution into eq 13 gives

$$\Delta A = \sqrt{\frac{kT}{\omega_s^2 m} + \frac{C^*}{12}\frac{4m+M}{2m+M}\frac{M}{m}r_o^2} \qquad (14)$$

This expression indicates that the amplitude dispersion at ion ejection is directly related to the effective ion temperature in the axial direction [13]. Additional consideration of velocity dispersion in the radial direction would allow $m(\Delta V)^2$ (similar to eq 12) to be related to the effective ion temperature as discussed in Mason and McDaniel [13]. This fact has additional implications for instrument resolution and spectral quality, which may be degraded by collision-induced dissociation of ions caused by scanning of the ions from the trap.

Minimum Ejection Line Width

Direct substitution into eq 1 of eq 14 along with eq 8 or 10 yields an expression for temporal line width Δt depending on the actual time of ion packet ejection t_{ej}. Although this substitution may be performed at any value, the primary interest is in the maximum obtainable resolution at a given scan speed that will occur at the minimum of Δt or the maximum of dA/dt.

At the point in time x_{ej} $(= a^{1/2}t_{ej})$ where the ion package is ejected, the amplitude of oscillation is given by $A(x_{ej}) = r_o/2^{1/2}$. Based on eq 5, this ejection point is determined by the excitation amplitude f_s, so that

$$f_s = \frac{\sqrt{2}\,\omega_s r_o\sqrt{a}}{F(x_{ej})} \qquad (15)$$

describes the excitation required to eject the ion packet at time x_{ej}.

To evaluate the maximum of dA/dt, eq 5 is differentiated with respect to t whereas eq 15 is substituted for f_s to obtain

$$\frac{dA}{dt} = \frac{r_o\sqrt{a}}{\sqrt{2}\,F(x_{ej})}\frac{dF(x_{ej})}{dx} = \frac{r_o\sqrt{a}}{\sqrt{2}}\frac{d\ln F(x_{ej})}{dx} \qquad (16)$$

dA/dt is proportional to the ratio of dF/dx to F. This ratio, also expressed as $d\ln F/dx$, is plotted for various values of $a^{1/2}\tau$ in Figure 2. Two different scalings are provided in this figure because the limiting case $a^{1/2}\tau \ll 1$ has a natural scaling of $a\tau t$, as seen in eqs 7 and 8, whereas the case $a^{1/2}\tau \gg 1$ scales to $a^{1/2}t$, as seen in eqs 9 and 10. At a given scan speed and damping, the maximum resolution depends on maximizing $d\ln F/dx$. This maximum occurs at $t_m = -1/a\tau$, as illustrated in Figure 2a, for all scan-rate and damping values! This result establishes the temporal shift of the ion ejection point (obtained at maximum resolution) relative to the resonant frequency of ion oscillations.

The maximum of dA/dt at ion ejection as a function of a and τ may be obtained for the two limiting cases on the basis of a similar evaluation as was performed to obtain eqs 8 and 10. For $a^{1/2}\tau \ll 1$, the rate of

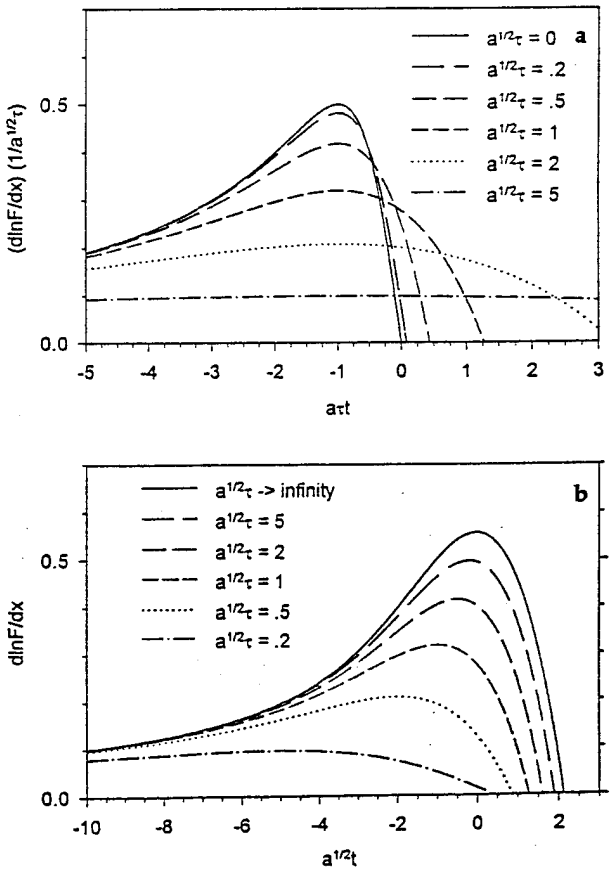

Figure 2. Derivative of the log of $F(x)$ for various scan-rate and damping factors as a function of $a\tau t$ and $a^{1/2}\tau$. All curves share a maximum at $a\tau t = -1$. The maximum on each curve indicates the optimum excitation amplitude and resolution.

Mass Dependence of Instrument Resolution

Equations 24 and 25 describe the mass dependence of the maximum obtainable resolution, but in fact both a and τ have mass dependence that should be made explicit. This affects both the resolution expressions of eqs 22 through 25 as well as appropriate axial excitation amplitudes discussed subsequently in eqs 37 through 40.

The mass dependence of a is straightforward: a is directly related to the mass scan rate via the differential form of eq 21 as seen in

$$a \equiv \frac{d\omega}{dt} = \frac{e\omega}{m}\frac{d(m/e)}{dt} \tag{26}$$

Although the frequency scan rate for a given mass-to-charge ratio remains constant over the course of the scan, the effective (frequency) scan rate decreases with increasing mass. This important result may be coupled immediately to eq 23 (high scan speed limit) to obtain

$$\frac{m}{\Delta m} = \left(m/2\sqrt{\frac{kT}{r_o^2\omega^2} + \frac{C^*M}{6}} \right)\sqrt{2\omega/e\pi\frac{d(m/e)}{dt}}$$

$$\sqrt{a}\,\tau \gg 1 \tag{27}$$

This result, where resolution is directly proportional to mass, may be used to illustrate clearly why unit mass resolution is readily maintained over the entire scan range of the "classic" ion trap [16, 17] system.

A brief qualitative argument illustrates this fact. It is well recognized that an ion trap that uses axial modulation [8] qualitatively gives resolution behavior similar to the classic mass-selective instability scan, whereas various researchers [10, 18, 19] have noted that line width behavior at higher q_z values (i.e., $q_z > 0.4$) should yield qualitatively similar characteristics. At the high q_z values (near $q_z = 0.9$) that are used for axial modulation, $kT < C^*Mr_o^2\omega^2/6$, so that in classic mass-selective instability at high scan speeds, eq 28 pertains:

$$\frac{m}{\Delta m} \propto m\Big/\sqrt{eM\frac{d(m/e)}{dt}} \qquad \sqrt{a}\,\tau \gg 1, kT \ll \frac{C^*}{6}Mr_o^2\omega^2 \tag{28}$$

The ion-mass m and neutral-molecule buffer-mass M [20] dependence of this expression are in good agreement with the known behavior of the classic mass-selective instability scan. The scan-rate dependence also agrees with high scan speed behavior described by Louris et al. [19] (see Figure 6a). This result further implies that resolution is independent of pressure if ions are sufficiently cooled prior to spectrum scanning [6, 7, 21].

Like a, τ also has mass dependence because $\tau = 2/c$ and c is defined in eq 11. In addition to the explicit terms, v_r and σ_D may also carry some mass dependence. The special case utilized by Goeringer et al. [10] involved an induced dipole-interaction model between the ion and the neutral molecules, because for this model, the collision frequency is truly independent of ion velocity in v_r. In such a case (by using $m \gg M$) we obtain

$$c = \frac{2\pi ne}{m}\sqrt{\frac{\alpha_p M}{\varepsilon_o}} \tag{29}$$

where α_p is the polarizability of the neutral and ε_o is the permittivity of free space.

The velocity independence of c is essential to the solution of eq 2 as presented in eqs 7 through 10. In this ion-induced dipole-interaction model, this velocity independence is preserved, although as seen in eq 11, the reduced collision frequency c in general depends on the relative velocity between the ion and a colliding neutral molecule. However, even in a more general ion-neutral interaction model, the relative velocity v_r (and therefore c) is still velocity independent if $kT \gg C^*Mr_o^2\omega^2/6$. This condition is the same as that which will be discussed subsequently as a temperature-limited resolution regime (see eq 32).

Nevertheless, this expression has some general applicability for lower mass ions, and utilizing eq 29, one may rewrite eq 22 as

$$\frac{m}{\Delta m} \simeq \frac{\sqrt{\varepsilon_o}\,\omega m^{3/2}}{\pi ne\sqrt{8a_pM}\sqrt{kT/r_o^2\omega^2 + C^*M/6}} \qquad \sqrt{a}\,\tau \ll 1 \tag{30}$$

This is the low scan speed analog of eq 27.

It must be noted that eqs 27, 28, and 30 all show a difference in resolution between ions of the same mass-to-charge ratio when these ions have different charge states. More explicitly, each equation can be written as a function of m/e multiplied by $m^{1/2}$. In this situation, the improvement in resolution for a multiply charged ion at a given m/e value is proportional to the number of elemental charges. It is important to note that this implies that under a fixed set of scanning conditions, the maximum mass resolution will be obtained for the singly charged ion.

The primary means of delineating the two operating regimes has been to consider the value of $a^{1/2}\tau$ relative to 1. This value also has an explicit mass dependence, based on eqs 26 and 29, as is given by

$$\sqrt{a}\,\tau = \frac{1}{\pi n}\sqrt{\left(\varepsilon_o\omega_m\frac{d(m/e)}{dt}\right)\Big/\alpha_p Me} \tag{31}$$

It is clear that the primary dependence in this expression is pressure, whereas all other factors are ex-

pressed as the square root. Nevertheless, under full scan experiments, the mass dependence does provide for differences of a factor of 3 or 4 for different ions in a given scan, yielding distinctive resolution behavior.

Temperature and Collisional Focusing

The effect of temperature on resolution arises from the ion packet dispersion term in the denominator of eqs 22 through 25. The dependence of resolution on temperature is governed by the relative values of the temperature itself and the frequency of supplemental excitation. The critical point occurs when

$$kT = \frac{1}{3}M\bar{V}_M^2 \simeq \frac{C^*}{6}Mr_o^2\omega^2 \qquad (32)$$

where V_M is the mean thermal velocity of the neutrals. This point occurs when the average axial ion velocity at ejection ($v_{rms} = r_o\omega/2$) exceeds the mean thermal velocity of the neutrals. For ejection frequencies (q_z values) below this critical point, the resolution is limited by the dispersion of the "stationary" ion packet before excitation, which is a function of system temperature and may be represented as

$$\frac{m}{\Delta m} \geq \frac{\sqrt{m}\, r_o\omega^2}{16\sqrt{2kT}} \frac{1}{\sqrt{\pi a}/2 + 1/\tau} \qquad kT \gg \frac{C^*}{6}Mr_o^2\omega^2 \qquad (33)$$

This expression clarifies that increases in ejection frequency greatly enhance the resolution until the condition of eq 32 is met. In a standard commercial ion trap mass spectrometry (ITMS) instrument (r_o = 1 cm, Ω = 6.911×10^6 s^{-1}) at 0°C, the condition of eq 32 is computed to occur at a supplemental frequency of 29.3 kHz (q_z = 0.075) for helium buffer gas and 11.1 kHz (q_z = 0.028) for nitrogen (assuming C^* = 1). Above these values, the increase in resolution with increasing frequency will be a modified linear relationship described by

$$\frac{m}{\Delta m} \geq \frac{(\omega/\sqrt{8})\sqrt{6m/C^*M}}{\sqrt{\pi a}/2 + 1/\tau} \qquad kT \ll \frac{C^*}{6}Mr_o^2\omega^2 \quad (34)$$

This is, of course, the opposite limiting case from eq 33. In this case, we see that buffer molecular mass becomes an important limiting factor in higher ejection frequency cases. In either case, increasing the ion mass or the excitation frequency yields increased resolution.

Figure 4 illustrates the relationship between temperature, buffer mass, and excitation frequency for five different buffer gases in both low and high scan speed limits. At low temperatures (the buffer-mass-limited case of eq. 28), the condition of maximum resolution is obtained, whereas increasing temperature provides a degraded resolution although the inflection point may

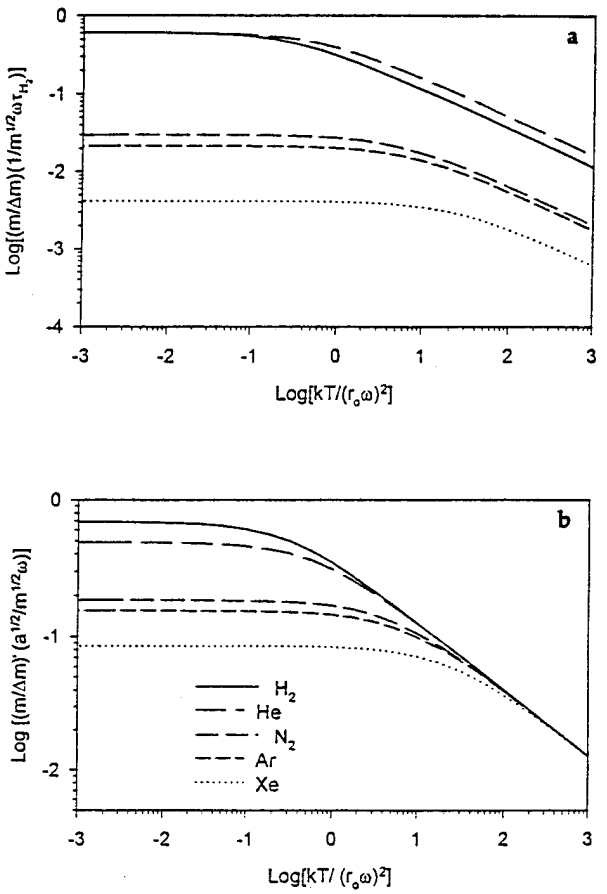

Figure 4. Temperature dependence of resolution for various buffer gases: (a) high scan speed limit $a^{1/2}\tau \gg 1$; (b) low scan speed limit $a^{1/2}\tau \ll 1$.

be varied by adjustment of the excitation frequency. One interesting feature of the low scan speed limit is the fact that helium rather than hydrogen provides the highest resolution. This is primarily due to the significantly lower polarizability (by more than a factor of 2) of helium.

The temperature of neutral buffer molecules has been used in the development of amplitude dispersion equations 12 through 14. This approach is consistent with the pseudopotential-well model developments of Major and Dehmelt [11]. It is clear that the actual ion temperatures reported in the literature [21–23], which are typically higher than the buffer ion temperature, depend also on the effective ion temperatures produced by non-thermal excitations of the ion trajectories. Several means for these excitations have been discussed including nonlinear resonances [9, 24], drive frequency harmonics [24], parasitic electrical signals, mechanical vibrations, and electrical noise [25].

Although these excitation sources must be recognized for their temperature-related effects in any ion chemistry experiment, it is clear that the hottest point for ions in virtually all ion trap experiments occurs at ion ejection. At ejection, the amplitude dispersion described by eq 14 has a direct thermal component and

an axial excitation component. The axial excitation component of this dispersion is proportional to the product $A\omega$, as was described in the derivation of eq 14, for each frequency component. As long as the $A\omega$ product for other non-secular oscillation frequencies is small with respect to $\tau_o \omega_s/2^{1/2}$, the dispersion factors for these other oscillations may be neglected in the spatial amplitude dispersion term.

Excitation Amplitude and Mass Shift

During the development of minimum ejection line width expressions, eq 15 described the relationship between the ejection point of the ion packet and the supplementary excitation amplitude. Further it was observed that dA/dt has a clear maximum for given a and τ values when the ejection point occurs at Δt_m as given by

$$\Delta t_m = -\frac{1}{a\tau} \tag{35}$$

(see Figure 2). This time is measured relative to the resonance point in the scan (e.g., $t = 0$ occurs at $\omega = \omega_s$). Substituting eqs 26 and 29 into this expression gives eq 36, which illustrates the effect of pressure, scan rate ($d(m/e)/dt$), and ejection frequency on the ejection time at maximum resolution:

$$\Delta t_m = -\left(\pi n \Big/ \left(\omega \frac{d(m/e)}{dt}\right)\right)\sqrt{\frac{\alpha_p M}{\varepsilon_o}} \tag{36}$$

This ejection time implies a mass shift that can be determined based on eq 21 to offer a comparison between mass shift and mass resolution. The relative mass shift at maximum resolution is given by

$$\frac{m}{\Delta m} = -\omega\tau = -\frac{\omega m}{\pi n e}\sqrt{\frac{\varepsilon_o}{\alpha_p M}} \tag{37}$$

which is independent of scan rate, but clearly dependent on ion mass-to-charge ratio, buffer mass, and pressure. For low scan speeds ($a^{1/2}\tau \ll 1$) this value may be directly compared to those in eqs 22 and 30.

This result is somewhat limited in that it only applies to the mass shift after the excitation amplitude f_s is adjusted to obtain maximum resolution. If the amplitude of the secular drive is not adjusted to yield maximum resolution for the ion mass of interest, it is clear that eq 15 will govern the mass shifts. The maximum delay possible in an ion ejection system occurs at the maximum value of amplitude envelope. In Figure 2 this corresponds to the point where $d \ln F/dx = 0$. At scan-rate extremes, ejection can only be delayed for a small time after resonance. For $a^{1/2}\tau \ll 1$, the maximum delay occurs approximately at $t = +2\tau$, whereas for $a^{1/2}\tau \gg 1$, the maximum delay occurs at about $t = +2/a^{1/2}$. By overdriving the axial excitation amplitude, ions may be ejected at any time prior to resonance, so that the minimum ejection time t is not limited by any boundary.

Because maximum resolution occurs at $x_m = -1/(a^{1/2}\tau)$, as seen in Figure 2, substitution of this value into eq 15 provides an expression for optimum excitation amplitude. Combined with the definition of f_s in eq 2, f_s can be directly related to the excitation voltage amplitude, so that

$$V_s = \frac{\sqrt{2}\, m r_o f_s}{e} = \frac{2\omega m r_o^2 \sqrt{a}}{F(-1/\sqrt{a}\,\tau)} \tag{38}$$

The behavior of V_s as a function of $a^{1/2}\tau$ is the inverse of the behavior of resolution in Figure 3. The value of V_s may be approximated in a manner similar to that for $m/\Delta m$ in eqs 24 and 25. The limiting cases are given by the expressions

$$V_s \geq \frac{2\sqrt{2}\,\omega m r_o^2}{e}\sqrt{\frac{1}{\tau^2} + \frac{a}{\pi}} \tag{39}$$

and

$$V_s \leq \frac{2\sqrt{2}\,\omega m r_0^2}{e}\left(\frac{1}{\tau} + \frac{\sqrt{a}}{\sqrt{\pi}}\right) \tag{40}$$

These expressions may again be substituted with eqs 26 and 29 to illustrate the mass dependencies at maximum resolution conditions. Further, substituting eq 26 for the case $a^{1/2}\tau \gg 1$ yields

$$V_s \approx 2\sqrt{2}\,\omega r_o^2 \sqrt{\frac{m\omega}{\pi e}\frac{d(m/e)}{dt}} \qquad \sqrt{a}\,\tau \gg 1 \tag{41}$$

whereas substituting eq 29 in the case $a^{1/2}\tau \ll 1$ yields

$$V_s \approx 2\sqrt{2}\,\omega \pi n r_o^2 \sqrt{\frac{\alpha_p M}{\varepsilon_o}} \qquad \sqrt{a}\,\tau \ll 1 \tag{42}$$

Of particular interest is the mass dependence of both expressions, which indicate that excitation frequency amplitudes may benefit from scanning in a manner similar to the rf scanning of the instrument. It should be noted that eq 41 describes a behavior that is qualitatively similar to that of a classical ITMS system for adjustment of the excitation amplitude relative to the scan rate and ion mass variables [26] and agrees well with ref 19 at 4.2 V.

This analysis is based on the assumption that a simple dipole field describes the electric field produced by the supplemental end cap voltages. Actual field values vary considerably from this dipole ideal. Even near the origin, correction values for the axial excitation electric field have been reported as 0.8 [27] and 0.877 [28] based on experimental and theoretical considerations, respectively. These dipole field correc-

tion values are a function of both radial and axial positions, and they are expected to be considerably smaller with radial displacements near the ring and to increase to unity near the center of the end caps.

Limitations and Comparison to Existing Theory

The present theoretical construction is an important departure from previous theoretical work [10] for three reasons. First, the high scan speed behavior is not dependent on pressure and proceeds as $a^{1/2}$ rather than $a\tau$ as in the previous analysis. It should be noted that this result is consistent with a large body of data that show resolution to be constant over a broad range of pressures when sufficient time is allowed to thermalize the ions before scanning [7, 22].

Second, the present theory predicts, via eqs 39 through 42, the excitation voltages required to obtain maximum resolution at any scan speed. However, we reiterate that important nonlinear field effects were disregarded in the derivation of these two equations. A correction factor is necessary to predict required excitation voltages accurately for a given resolution; one correction factor is probably obtained best from experiment, but the scan-rate dependencies and temporal line shifts should not be altered by these considerations.

Third, the ion dispersion description implies that resolutions are directly dependent on the relative masses of the buffer neutrals and the ions themselves owing to collisional focusing. Furthermore, this effect is independent of the scan-rate regime. This effect describes how higher resolutions are produced for higher masses in any continuous scan. This term also incorporates the effects of temperature (and, qualitatively, electrical noise) into the consideration of resolution.

Figure 5 illustrates a predicted resolution comparison between the present result and the previous frequency line width mode [10]. The resolution predicted in the present theory is actually higher in both scan-rate regimes. In the slow scan regime the resolution is higher owing to the collisional focusing of the higher mass ions by the light neutrals. This focusing effect is also present at high scan speeds, but it is more important to note that the $1/a^{1/2}$ behavior of the resolution implies higher resolution even without this focusing effect.

Note that several important sources of amplitude dispersion have been neglected in the present theory to focus on the ion behavior in a damped harmonic oscillator model. During the previous discussion of temperature, electrical noise was dismissed as a major source of spatial ion packet dispersion, but temporal and frequency dispersion effects, which could result from noise in the radiofrequency drive or other electrical and mechanical sources, were not considered. It is worth noting that $\Delta\omega_s$ is directly proportional to ΔV in the drive voltage and that this may yield significant

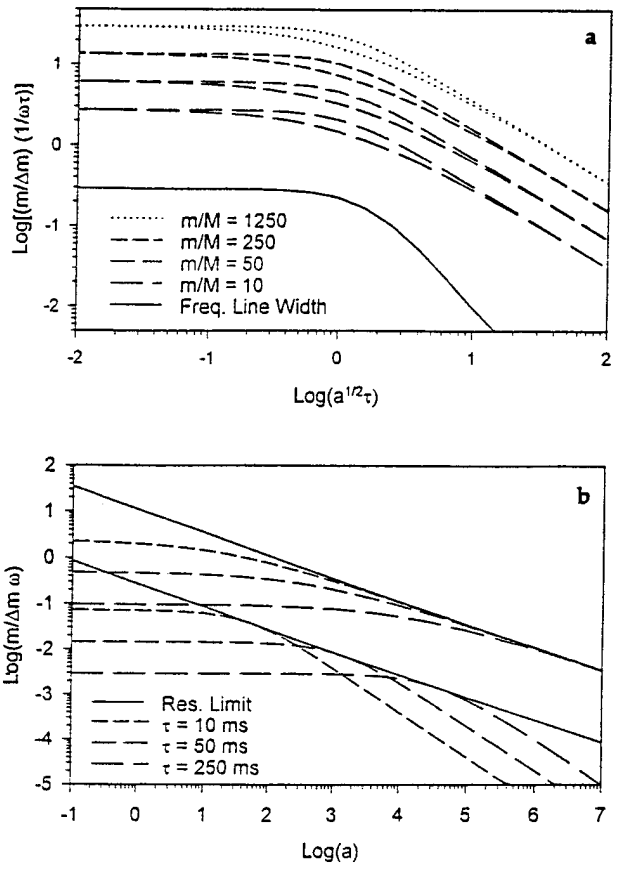

Figure 5. (a) Comparison of mass resolution at four different m/M values in the low temperature limit. Both upper and lower bounds are shown. The behavior of the previous frequency line with model is also shown for comparison. (b) Specific comparison of the present model at $m/M = 125$ with the existing frequency line width model. The upper four broken curves illustrate the present model at three damping factors, whereas the lower 3 illustrate the frequency line width model of the same three values. The two solid lines indicate the maximum obtainable resolution as a function of scan rate for the two models.

temporal fluctuations in the amplitude of the ion packet during scanning.

Geometrical considerations also have been neglected. In a standard commercial instrument, the axial position that corresponds to the ion exit aperture is a function of radius. If the exit aperture is only 3.5 mm in radius, the ΔA of the aperture may be as large as $0.04r_o$, which is the same as collision-based dispersion produced by an m/M ratio of 92 (e.g., m/z 370 in He buffer) in the low temperature limit. Clearly for higher masses the aperture size could easily be the resolution-limiting element.

Geometrical variations already mentioned with respect to the supplemental axial excitation field will also reduce resolution because the effective excitation voltage is a function of radius in the trap. This second effect has the potential to be more important than the first, given the strong radial dependence of the excitation field strength already discussed. It is our opinion that these geometrical effects are the dominant resolu-

tion-limiting effects for high mass analyses in commercial instruments. A full accounting of these geometrical effects is beyond the scope of this article, but it is clear that both effects may be mitigated by use of small apertures, which limit ion detection to those trajectories near the axis of symmetry.

Implications for High Mass Analyses

The driving force behind examinations of ion trap resolution in mass-selective instability scans has been attempts to obtain high resolution mass spectra at very high mass-to-charge ratios [10, 29]. Because a given instrument is generally limited to a maximum operating voltage either by electrical discharge or engineering constraints, three means have been used to extend the mass range of the ion trap to allow ejection of high mass ions: reduction of the resonance ejection operating point q_z [5, 30], reduction of the operating frequency Ω [31, 32], and reduction of the trap radius r_o [31, 32]. When one or more of these means is coupled with slow scan speeds, a combination of high mass analysis and high resolution may be obtained.

Use of any one of these three means to expand the mass range results in temperature-limited resolution because $kT \gg C^*Mr_o^2\omega^2/6$. In the case of this limit, eq 32 may be rewritten as

$$\frac{m}{\Delta m} \simeq \frac{\sqrt{\varepsilon_o}\, r_o (q_z\Omega)^2 m^{3/2}}{16\pi ne\sqrt{2\alpha_p MkT}} \qquad \sqrt{a}\,\tau \ll 1, kT \gg \frac{C^*}{6} Mr_o^2\omega^2 \tag{43}$$

which is the primary resolution expression for high mass analyses.

The $m^{3/2}$ dependence in eq 43 indicates promising resolution possibilities, but is in itself misleading. If the operating voltage could increase without limit, this would describe the mass dependence of resolution. In practice, the highest mass-to-charge ratio detectable is directly proportional to the maximum operating voltage according to the definition of q_z in eq 2. Substitution of the q_z expression into eq 43 allows expected resolution at high masses to be written as

$$\frac{m}{\Delta m} \simeq \frac{\sqrt{\varepsilon_o}\, eV^2}{\pi n r_o^3 \Omega^2 \sqrt{2\alpha_p mMkT}}$$

$$\sqrt{a}\,\tau \ll 1, kT \gg \frac{C^*}{6} Mr_o^2\omega^2 \tag{44}$$

Equation 44 clarifies that once the maximum value of V has been reached, resolution as expected decreases with increasing mass because the operating point q_z must be reduced to extend the mass range of the instrument.

It is not clear that reductions in r_o or Ω in eq 44 are accompanied by an increase in the operating point and that this procedure may only continue until a maximum effective operating point for the trap is reached. This maximum effective value from other experiments appears to be $q_z = 0.73$ [10, 18] rather than the expected stability limit of $q_z = 0.91$.

A clear impression of the maximum possible resolution at high mass may be obtained by a different substitution of q_z into eq 43. Substituting for the product $r_o\Omega^2$, we obtain

$$\frac{m}{\Delta m} \simeq \frac{\sqrt{\varepsilon_o m}\, q_z (V/r_o)}{4\pi n\sqrt{2\alpha_p MkT}} \qquad \sqrt{a}\,\tau \ll 1, kT \gg \frac{C^*}{6} Mr_o^2\omega^2 \tag{45}$$

which describes the maximum possible resolution for an ion of mass m at operating point q_z. The ratio V/r_o comes from electrical-discharge considerations and represents a maximum value that is related to a maximum electric field strength. It is also important to notice that this result is independent of the electrical charge of the ion.

It is important to recognize that this result is based on the temperature-limited regime, but that reductions in operating frequency actually increase the secular frequency ω so that the $kT \gg C^*Mr_o^2\omega^2/6$ condition may be altered. It is also important to note that a similar evaluation of eq 33 to describe the maximum possible resolution for any ion is more difficult and beyond the scope of this paper.

The analysis that produced eqs 43 through 45 utilized the ion-induced dipole-interaction model. Once an ion is sufficiently large, the probability that a neutral molecule will interact with the charge center rather than a neutral portion of the ion structure becomes increasingly small. The ion-neutral interaction radius is given by

$$b_o^2 = \frac{2e}{v_r}\sqrt{\frac{\alpha_p}{\varepsilon_o M}} \qquad m \gg M \tag{46}$$

When the ion dimensions are on the order of b_o, we may expect that a hard-space-type scattering model will take over, so that the mass dependence of c, as per eq 11, will relate to the molecular cross section of the ion (i.e., σ_D is proportional to $m^{2/3}$). Once this limit is reached, the analog on eq 43 becomes

$$\frac{m}{\Delta m} \propto \frac{r_o (q_z\Omega)^2 m^{5/6}}{n\sqrt{kT}} \qquad \sqrt{a}\,\tau \ll 1, kT \gg \frac{C^*}{6} Mr_o^2\omega^2 \tag{47}$$

for very large m. Similar analogies to eqs 44 and 45 indicate that resolution decreases with increasing mass (once the voltage limit is reached) by factors of $m^{-7/6}$ and $m^{-1/6}$, respectively.

Ultimately the improvement of resolution will cease to keep up with the increasing mass. By using values

for the polarizability of N_2 and He included in Mason [13], we can show that the collision radius b_0 is 12.5 Å for N_2 and 7.3 Å for He with respect to a singly charged ion. These values are easily exceeded by the dimensions of a singly charged ion at 10,000 u, so that expected resolutions for such high mass ions will require extremely low pressures to compensate for the less favorable hard-sphere-type interaction conditions.

Beyond the Pseudopotential-Well Approximation

At several times during this discussion, we alluded to behavior of resonance ejection scans for q_z values beyond the 0.4 limit of the pseudopotential-well approximation. This is of course because the resonance phenomena themselves are still active at these higher q_z values [8, 9]. Furthermore, we believe there is nothing conceptually flawed about the use of this description at higher q_z values if appropriate considerations are developed. It is for this reason that we have typically utilized ω rather than $q_z\Omega$ in resolution (and other) expressions so that they may be extended to high q_z values.

The first consideration that must be addressed to extend the present work beyond the pseudopotential-well region is the use of a harmonic oscillation model to determine the amplitude dispersion in eq 14. Outside the pseudopotential region, v_{rms} as used in eq 13 is no longer accurate because harmonic components of the oscillation make important contributions to the rms velocity. Therefore ΔA as developed in eq 14 is typically too small at high q_z values. This should be compared to the results of Louris et al. [19], which indicate resolution decreases for q_z values above 0.73.

Second, the use of eq 1 implies a more basic assumption; this is, the amplitude distribution is unchanged during the scanning of the mass peak. At high scan speeds (i.e., $a^{1/2}\tau \gg 1$) this is clearly true, but at low scan speeds, additional questions are raised. In effect, ions may "diffuse" from low to high amplitude regions of the distribution because of collisions with neutrals. This diffusion occurs at a rate that is proportional to the reduced collision frequency times the width of the distribution. Therefore as long as eq 48 is obeyed,

$$\frac{dA}{dt} \gg c\,\Delta A \tag{48}$$

the distribution will remain largely unchanged during scanning. It is interesting to note that by substitution this expression can be shown to be equivalent to the condition $a^{1/2}\tau \gg 1$.

At low-scan speeds, this implies that the ions may actually "diffuse" out of the trap prior to the normal ejection point of the distribution. In other words, most ions will enter a sufficiently high trajectory for ejection prior to the time when the bulk of the unaltered distribution would have reached the edge of the trap aperture. This effect may alter the ejection time for ions, but it does not alter the peak width because the relaxation time τ is proportional to $\Delta A/(\delta A/\delta t)$ in the pseudopotential-well region and in a diffusive ejection process, the peak width is also proportional to this relaxation time.

At high q_z values the rate at which ions may change amplitude trajectories is altered by a secondary effect. The oscillation amplitude now is based on a superposition of multiple frequencies. Without collisions the phase relationship between the secular and trapping frequencies is determined by the voltages driving the oscillations and the initial conditions, but the presence of collisions may alter the phase relationship between the two oscillation frequencies. If the different oscillations have amplitudes on the same order of magnitude, it is clear that minor changes in phase due to collisions may produce alterations in amplitude on the order of ΔA from a single collision. In other words, the collision frequency of the ions with individual neutrals may determine the rate at which ions diffuse out of the trap at lower scan speeds. Therefore the actual collision frequency c' described by

$$c' = nv_r\sigma_p = \frac{m + M}{M}c \tag{49}$$

determines the relaxation time constant τ', and the temporal line width Δt may be expressed as the smaller of eq 20 and $\tau' \equiv 4c'$.

These additional caveats are added to the previous geometrical considerations. Figure 6 illustrates a comparison between theoretical predictions and recent experimental results published by the Finnigan group (Louris et al. [19]) and by Loundry et al. [3]. Both sets of results illustrate resolutions between 2 and 4 orders of magnitude greater than the frequency line width model predicts. Figure 6a compares the maximum resolution prediction of the present model to values obtained by Louris et al. [19] for the m/z 129 ion of xenon ejected at $q_z = 0.73$. It already has been noted that a voltage prediction of 4.2 V to obtain maximum resolution agrees very well with the value of ~ 5 V obtained by Louris et al. [19] at a scan rate of 5500 u/s. It should be noted that eq 41 predicts that maximum resolution will be obtained at V_s values beyond the capability of the commercial instrument for higher mass ions ($m/z > 100$). Resolution improvements for high mass ions produced by using axial excitation voltages between 6 and 25 V were recently demonstrated in our laboratory [26].

Figure 6b compares predictions of the present model with results recently reported by Loundry et al. [3]. The lack of $a^{1/2}$ dependence (which is indicated by the solid line), the lack of mass dependence, and the fact that that present theoretical construction still underestimates the resolution line by a factor of 10 are of considerable concern. The authors believe this is due to

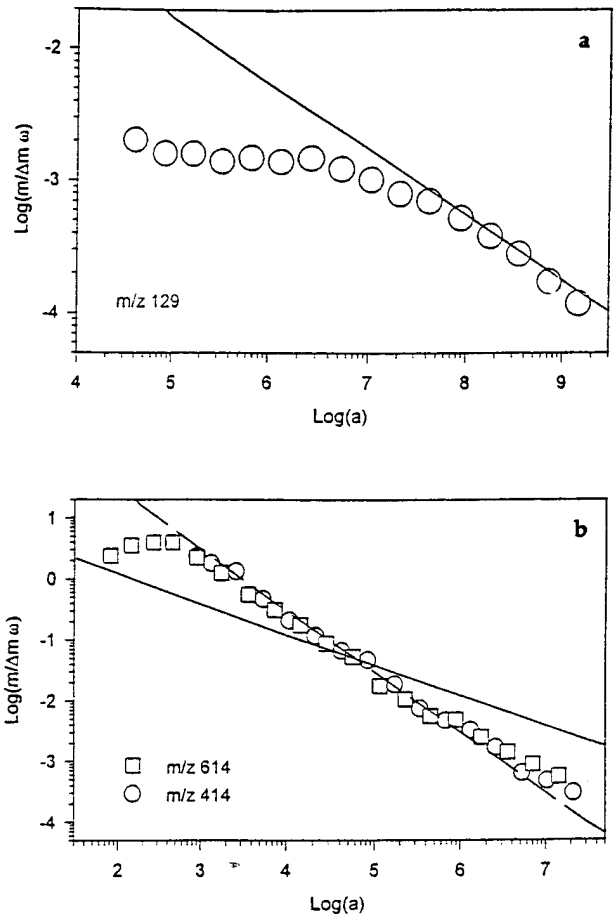

Figure 6. Comparison of the present model with results obtained by (a) Louris et al. (19) and by (b) Loundry et al. (3). The solid line indicates predicted maximum resolution. Additional details are in the text.

a collection of the previously mentioned secondary effects. The dotted line in this figure corresponds to

$$\frac{m}{\Delta m} = \frac{\omega c'}{2a} \tag{50}$$

This is the expected scan-rate dependence when the temporal line width is determined by the collision relaxation time τ'. In this case, we took the pressure to be 10^{-4} torr and temperature to be 300 K. The highest resolution is obtained at $a^{1/2}\tau \simeq 1$ in this curve, and the peak width is determined by the τ' until eq 20 again becomes the limiting expression for line width. At the higher scan speeds, the $a^{1/2}$ dependence returns, but the resolution is less than predicted because of (at least) two factors we have already mentioned: (1) the geometrical considerations in aperture shape and dipole excitation and (2) limitation of excitation amplitudes to 6 V on commercial instruments. Two reasons for not observing this same phenomenon in Figure 6a also should be noted: (1) the lower q_z value in the Louris et al. [19] data reduces the drive frequency amplitude with respect to secular amplitude and (2) the initial amplitude dispersion is wider for the lower mass ions.

Conclusion

The present amplitude-dispersion-based additions to the frequency line-width-based model of Goeringer et al. [10] offer considerable insight into the phenomena that affect resolution in ion-trap-based instruments. Furthermore, it appears to do so at high scan speeds and q_z values that are beyond the limiting cases used in the construction of the theory, even though considerable effort may be required to develop the appropriate correction values required to make the theory quantitative for predictions in these regions. Ongoing efforts by other researchers in the areas of temperature estimation [21–23], nonlinear resonances [9, 24], and ion trajectory studies [33, 34] as well as additional efforts in the areas of geometrical issues [27, 28] and collisional effects [33, 34] on ion packet trajectories will all contribute to the ultimate understanding of ion trap resolution properties.

Acknowledgments

This work was sponsored by the Army Research Office under contract DAAL03-91-G-0296.

References

1. Paul, W.; Reinhard, H. P.; Von Zahn, U. *Z. Phys.* **1958**, *152*, 143.
2. Williams, J. D.; Cox, K.; Morand, K. L.; Cooks, R. G.; Julian, R. K.; Kaiser, R. E. In *Proceedings of the 39th ASMS Conference on Mass Spectrometry and Allied Topics*, Nashville, 1991; p 1481.
3. Loundry, F. A.; Wells, G. J.; March, R. E. *Rapid Commun. Mass Spectrom.* **1993**, *7*, 43.
4. Kaiser, R. E., Jr.; Cooks, R. G.; Stafford, G. C.; Syka, J. E. P.; Hemberger, P. H. *Int. J. Mass Spectrom. Ion Process.* **1991**, *106*, 79.
5. Kaiser, R. E.; Louris, J. N.; Amy, J. W.; Cooks, R. G. *Rapid Commun. Mass Spectrom.* **1989**, *3*, 225.
6. Kelley, P. E.; Stafford, G. C.; Stephens, D. R. U.S. Patent 4,540,884, September 10, 1985.
7. March, R. E.; Hughes, R. J. In *Quadrupole Storage Mass Spectrometry*; Winefordner, J. D.; Kolthoff, I. M., Eds.; Chemical Analysis Series 102; Wiley: New York, 1989.
8. Syka, J. E. P.; Louris, J. N.; Kelley, P. E.; Stafford, G. C.; Reynolds, W. E. U.S. Patent 4,736,101, 1988.
9. Franzen, J.; Gabling, R.-H.; Heinen, G.; Weiss, G. U.S. Patent 4,882,484, November 21, 1989.
10. Goeringer, D. E.; Whitten, W. B.; Ramsey, J. M.; McLuckey, S. A.; Glish, G. L. *Anal. Chem.* **1992**, *64*, 1434.
11. Major, F. G.; Dehmelt, H. G. *Phys. Rev.* **1968**, *170*, 91–107.
12. Marion, J. B. *Classifcal Dynamics of Particles and Systems*; Academic Press: New York, 1970; p 117.
13. Mason, E. A.; McDaniel, E. W. *Transport Properties of Ions in Gases*; Wiley Interscience: New York, 1988; p 144.
14. Gautschi, W. In *Handbook of Mathematical Functions*; Abramowitz, M.; Stegun, I. A., Eds.; Dover: New York, 1972; pp 295–330.
15. Fowles, G. R. *Introduction to Modern Optics*; Holt, Rinehart, and Winston: New York, 1975; pp 125–135.

16. Stafford, G. C.; Kelley, P. E.; Syka, J. E. P.; Reynolds, W. E.; Todd, J. F. J. *Int. J. Mass Spectrom. Ion Process.* **1984**, *60*, 85.
17. Weber-Grabau, M.; Kelley, P. E.; Bradshaw, S. C.; Hockmann, D. J. In *Proceedings of the 36th ASMS Conference on Mass Spectrometry and Allied Topics*, San Francisco, 1988; p 1106.
18. Schwarz, J. C.; Syka, J. E. P.; Jardine, I. *J. Am. Soc. Mass Spectrom.* **1991**, *2*, 198.
19. Louris, J.; Freuler, S.; Kirkish, J.; Schwartz, J.; Statford, G.; Syka, J.; Taylor, D.; Tucker, D.; Zhun, J. In *Proceedings of the 39th ASMS Conference on Mass Spectrometry and Allied Topics*, Nashville, TN, 1991; p 542.
20. Cameron, D.; Hemberger, P. H.; Alarid, J. E.; Liebman, C. P.; Williams, J. D. *J. Am. Soc. Mass Spectro.* **1993**, *4*, 774.
21. Vedel, F. *Int. J. Mass Spectrom. Ion Process.* **1991**, *106*, 33.
22. Wu, H.-F.; Brodbelt, J. S. *Int. J. Mass Spectrom. Ion Process.* **1992**, *115*, 617.
23. Basic, C.; Eyles, J. R.; Yost, R. A. *J. Am. Soc. Mass Spectrom.* **1992**, *3*, 716.
24. Vedel, F.; Vedel, M.; March, R. E. *Int. J. Mass Spectrom. Ion Process.* **1990**, *99*, 125.
25. McLuckey, S. A.; Goeringer, D. E.; Glish, G. L. *Anal. Chem.* **1992**, *64*, 1455.
26. Arnold, N. S.; McClennen, W. H.; Meuzelaar, H. L. C. In *Proceedings of the 41st ASMS Conference on Mass Spectrometry and Allied Topics*, San Francisco, CA, 1993; p 21a.
27. Philip, M. A.; Gelbard, F.; Arnold, S. J. *J. Colloid Interface Sci.* **1980**, *75*, 566.
28. Davis, E. J. *Langmuir* **1985**, *1*, 379.
29. Cooks, R. G.; Amy, J.; Bier, M.; Schwartz, J.; Schey, K. *Adv. Mass Spectrom.* **1989**, *11A*, 33.
30. Fulford, J. E.; Hoa, D.-N.; Hughes, R. J.; March, R. E.; Bonner, R. F.; Wong, G. L. *J. Vac. Sci. Technol.* **1980**, *17*, 829.
31. Kaiser, R. E.; Cooks, R. G. *Rapid Commun. Mass Spectrom.* **1989**, *3*, 50.
32. Kaiser, R. E.; Cooks, R. G.; Moss, J.; Hemberger, P. H. *Rapid Commun. Mass Spectrom.* **1989**, *3*, 50.
33. Williams, J. D.; Cooks, R. G.; Syka, J. E. P.; Hemberger, P. H.; Nogar, N. S. *J. Am. Soc. Mass Spectrom.* **1993**, *4*, 792.
34. Loundry, F. A.; Alfred, R. L.; March, R. E. *J. Am. Soc. Mass Spectrom.* **1993**, *4*, 687.

U.S.-HUNGARY SCIENCE & TECHNOLOGY PROGRAM - PROJECT PROPOSAL COVER PAGE

1. Date received: _____ (for JF Secretariat use)

2. JF ID Number: _____ (for JF Secretariat use)

3a. Title of Proposed Project: Characterization of Aerosol Particles by means of Quadrupole Ion Trap

3b. Short Identification Title: Aerosol Characterization

4a. Activity Type: Research Project + Conference/Workshop: ___ Project Development Visit: ___

4b. Years Duration: 3

HUNGARIAN PRINCIPAL INVESTIGATOR	U.S. COUNTERPART SCIENTIST
5a. Name: Hárs György Dr (LAST NAME First MI Degree)	5b. _____ (LAST NAME First MI Degree)
6a. Title: Ass. Prof.	6b. _____
7a. Institution: Department of Atomic Physics	7b. _____
8a. Address: Technical University of Budapest 1111 Budapest, Budafoki u. 8. HUNGARY	8b. _____
9a. Telephone: (361) 166-6075	9b. _____
10a. Fax: (361) 185-3230	10b. _____

SIGNATURES AND INSTITUTIONAL APPROVALS

11a. Signature: _____ Hungarian Principal Investigator

11b. _____ U.S. Counterpart Scientist

12a. Signature: _____ (Hungarian Institutional Director/Fiscal Officer)

12b. _____ (U.S. Institutional Director/Fiscal Officer)

13a. Name: Dr. Richter Péter

14a. Title: Head of Department

13b. _____

14b. _____

15. Summary of Proposed Budget

	Year One Forints	One Dollars	Year Two Forints	Two Dollars	Year Three Forints	Three Dollars	3 Years Forints	Total Dollars
15a. Total costs	940.000	9.870	886.000	9.720	920.000	9.760	2.746.000	29.350
15b. Adjustment								

Technical University of Budapest
Department of Atomic Physics

Budafoki út 8. Budapest, H-1111, Hungary
Phone: (361) 185-3230 or
(361) 166-4011/15-87
Fax: (361) 185-3230
Telex: 225931 muegy h

Statement of Work

In the joint project "Aerosol Characterization by means of Quaqrupole Ion Trap" funded by the U.S. Hungarian Joint Fund, the University of Utah has the following commitments:

1. Make possible a visit to Budapest for the U.S. principal investigator,

2. Providing access to the ion trap equipment for the Hungarian principal investigator during his visit at University of Utah.

Both the above commitments are financed by the proposed budget (see Travel costs)

Dr. Gyorgy Hars

Principal Investigator